FEBRUARY 1983

LRP 220/83

A SPECTROSCOPIC SURVEY OF THE TCA TOKAMAK WITH AND WITHOUT LOW-FREQUENCY RF HEATING

M.F. Stamp, A. Pochelon, N.J. Peacock,
J.B. Lister, B. Joye, H. Gordon

A SPECTROSCOPIC SURVEY OF THE TCA TOKAMAK WITH AND WITHOUT LOW-FREQUENCY RF HEATING

H. Gordon", N.J. Peacock, M.F. Stamp+
Culham Laboratory
UKAEA - Euratom
Abingdon, England

B. Joye, J.B. Lister, A. Pochelon
Centre de Recherches en Physique des Plasmas
Association Euratom - Confédération Suisse
Ecole Polytechnique Fédérale de Lausanne
CH-1007 Lausanne - Switzerland

ABSTRACT

A spectrographic survey of the impurity lines between 250-3000 Å was made on the TCA tokamak both with and without additional rf power input. The wavelength precision of the important diagnostic lines of the ionised metals, chromium, iron and nickel, has been improved. In particular the 3s-3p transitions in magnesium-like and sodium-like ions and the 2s-2p transitions in fluorine-like and oxygen-like ions of the metals have been revised. Doping of the tokamak plasma with neon, oxygen and nitrogen permitted accurate measurements of the helium-like 1s2s - 1s2p transitions to be made and compared with recent quantum electrodynamic calculations. In the photoelectric mode the temporal behaviour of accessible oxygen and iron lines has been documented during tokamak discharges with additional rf power, during which period there is a large increase in the radiated power loss. The spectroscopic and bolometric data have been correlated. Estimates of the iron concentration show that it increases and becomes more peaked on axis during the rf pulse.

" University of Strathclyde, Scotland
+ Oxford University, England

I. INTRODUCTION

TCA is a modest sized tokamak, described in detail by CHEETHAM et al. (1980 a, 1980 b). Its main characteristics are

$R, a = .61, .18$ m

$B_\phi = 7.6 - 15.1$ kG

$I_p \leq 140$ kA

$n_e \leq 9.5\ 10^{19}\ m^{-3}$ in H_2 or D_2

The experiment was conceived to study Alfvèn Wave Heating at frequencies $\omega < \omega_{ci}$ and results on the first low power experiments are described by DE CHAMBRIER et al. (1982 a, 1982 b). The torus is ungettered and was polished during manufacture. Discharge cleaning is carried out each evening using 20 msec pulses at 5 kHz, three per second, known generically as Taylor Cleaning. The tokamak has a wide operating range between $q = 2.2$ and $q = 20$. It was commissioned in June 1980, rf experiments were started in March 1981, and power heating experiments were begun in March 1982. The first Alfvèn Wave Heating results have been described by DE CHAMBRIER et al. (1982 c, 1982 d).

The rf antenna system is composed of a set of discrete structures. Each antenna group consists of three plates; one group is placed above and another below the plasma in each of the four quadrants of the torus. The antennae themselves float with respect to the vessel, and are characterized by a low impedance, leading to high antenna currents and low antenna voltages. We have only used unscreened antennae to date and have not observed any arcing or other breakdown

problems. The frequency used for all the work described here was 2.67 MHz. The first results showed electron and ion heating accompanied by a considerable increase in the radiated power loss during the rf pulse together with an increase in plasma density, an increase in the plasma resistance and a subsequent reduction in the plasma duration. These problems led us to carry out a spectroscopic survey of the TCA Tokamak, with and without rf heating, to identify the dominant impurities. In addition we profited from the presence of a high resolution spectrometer by carrying out some basic spectroscopic measurements, including studies of impurity-doped plasmas. In Table I we list the photographic exposures, along with the varying tokamak conditions in which they were made.

In Section II we describe the apparatus. In Sections III-VI we discuss the general features observed and the precision photographic wavelength measurements. In Section VII we report on the measurements made photoelectrically and their relation to the bolometric measurements, and finally, in Section VIII, we estimate the iron impurity concentration before and during the rf pulse.

II. SPECTROSCOPIC APARATUS

A 1-metre normal incidence concave diffraction grating spectrometer (Rank-Hilger Model E766) viewed a fixed chord of the plasma in the horizontal median plane and along a major radius, which is displaced 45^0 away from the stainless steel limiters. The instrument was capable of covering the spectral region between 2800Å and 250Å both photogra-

phically and photoelectrically. The single channel TPB phosphor-photomultiplier detector could conveniently be interchanged with the photographic film holder so that their detailed time history during the discharge as well as any long term changes in the overall impurity constituents could be readily checked during the 2-3 month duration of the experimental programme.

Three different diffraction gratings were used in order to maximise the spectrometer efficiency over the wide wavelength range studied. Platinum coated 1200 ℓ/mm gratings blazed at 450Å and 1500Å were used to cover the short and long wavelengths respectively, while an osmium coated 2400 ℓ/mm grating blazed at 1350Å was used at intermediate wavelengths and for all the high resolution measurements.

In the photographic mode, the entrance slit width was varied from a minimum of 15 μm, to resolve the many close calibration lines and to aid identification using the variation in the Doppler widths of the lines, up to a maximum of 50 μm, to increase the relative intensity of the wide Doppler-broadened lines. A mechanical shutter before the entrance slit was used to expose the film to just the central period of most of the discharges, with integrated exposure times varying from 1/4 to 2 seconds.

III. MAIN FEATURES OF THE VUV SPECTRUM

Plates 1-8 show the VUV radiation emitted by impurities in the TCA tokamak plasma from 280Å - 2740Å. All of the strongest lines are identified, and appear in several orders of diffraction. Some weak

lines are not positively identified, both because the order of the lines may not be clear, and because the wavelength finding tables are incomplete. The impurity spectrum can be separated into three main regions:

(a) $\lambda > 1900$Å - Low ionisation states of the metal ions, eg Fe II, Fe III, Cr II, Cr III, are predominant, though the low charge states of carbon, nitrogen and oxygen are also intense.

(b) $450 < \lambda < 1900$Å - Most lines are emitted from Low Z impurities, although some forbidden (M2) lines from highly-ionised metals are also present.

(c) $280 < \lambda < 450$Å - Incompletely stripped low Z ions emit some lines in this wavelength range, but most of the radiation is from quite high states of the metal impurities, eg Fe X to XVI.

The 2s-2p Li-like and 3s-3p Na-like resonance transitions are generally the most easily observed of any of the multiplets emitted by ionised impurities. Hence, a simple technique for identifying the impurities present in the plasma is to search for the 2s-2p and 3s-3p doublets on the exposed photographic films. In this way, it is readily seen that Fe, Cr, C, N, and O are the main TCA impurities, but some Ni and Si, and even smaller amounts of Ar, Al, Na, F and S are also present.

Fig. 1 indicates the temperature at which a few important impurity species might be expected to dominate in equilibrium conditions of the ionisation-recombination balance. In the VUV region of the

spectrum, however, the only multiplet of the H- and He-like ion species to manifest itself is the $1s2s\ ^3S_1$ - $1s2p\ ^3P_{2,1,0}$. In the present study this multiplet was not observed in elements higher than neon. The 2s-2p Li-like doublet on the other hand was readily identifiable in elements up to argon while the 3s-3p Na-like emission was a strong feature in all the metallic elements present.

IV. PRECISION WAVELENGTH MEASUREMENTS

The photographic records of the spectra were of sufficiently high quality to allow accurate (10 ppm) wavelength measurements to be made. Low ionisation states of carbon, nitrogen, oxygen and iron in the TCA tokamak emit line radiation the wavelengths of which are documented with some precision, typically $\delta\lambda < \pm$ 0.002Å (see KAUFMANN and EDLEN (1974)) . These low charge states emit throughout the observed spectral region and are used as convenient "transfer standards" for measuring the wavelengths of the less well known multiplets in more highly ionised atoms.

Precision wavelengths are particularly topical for the $n = 2 \rightarrow 2$ and $n = 3 \rightarrow 3$ transitions of the common metals where forbidden transitions within the ground configuration of the ions and intersystem lines are widely used as diagnostic indicators in both solar and fusion plasma research. As a result of this present study, improved values of wavelengths in the elements Ar, Cr, Fe, Ni are made available. Previously (eg FAWCETT (1970), WIDING and PURCELL (1976)),the metal lines have been measured from photographic plates of the

solar spectrum to only about 50 ppm, while photoelectric measurements of tokamak emission (eg HINNOV (1979)) had a precision limited typically to about 150 ppm.

Multiplets for which improved wavelengths have been derived in the present study include the intercombination $3s^2\ ^1S_0$ - $3s3p\ ^3P_1$ magnesium sequence, the $3s\ ^2S$ - $3p\ ^2P$ sodium sequence, the $2s^2 2p^5\ ^2P_{3/2}$ - $2P_{1/2}$ fluorine sequence and the $2s^2 2p^4\ ^3P_2$ - $^3P_1$, $^1D_2$ oxygen sequence.

It might well be asked why such multiplets cannot be derived from ab initio atomic structure calculations. In many-electron ions and atoms, electron correlations, relativistic and radiative corrections are difficult to calculate precisely, so that large, though usually systematic, discrepancies occur between theory and experiment. However, improved "theoretical" wavelengths can be generated semi-empirically by assuming a smooth variation of this discrepancy along an isoelectronic sequence as in the work of EDLEN (1982).

The present measurements indicate that for the 3s-3p Na-like, 2s-2p Li-like and the $2s^2 2p^5$ ($^2P_{3/2}$ - $^2P_{1/2}$) F-like isoelectronic series, a better extrapolation can be made using these new tokamak observations. For example, the discrepancy between theory and experiment for the F-like sequence scales nearly as Z^3. Fig. 2 shows the quantity (experiment-theory)/Z^3, plotted against Z, and demonstrates that the previous best extrapolation by ELDEN (1982) is inaccurate at high Z, due to the large errors for these ions in the previous measurements. It can be seen that the new TCA and DITE tokamak observations are internally consistent, and they suggest a new "best fit" that

that differs by up to 0.2Å from the previous data. It is clear that the old calcium wavelength misled the previous extrapolation, and should be remeasured.

V. EMISSION LINE PROFILES

The resolution of the normal incidence spectrometer using the 2400 ℓ/mm grating and with photographic recording is adequate to record differences in the thermal widths of the emission lines. Inspection of Figs. 3 and 4 indicates relatively large broadening of the high ionisation potential ions, N VI and Ne IX for example, under ohmically heated plasma conditions. Unfolding the instrument function, as measured by the widths of the lines from the low ion stages eg Fe III, Fig. 3, from the more severely broadened highly-ionised emission, yields the half-widths of the latter due to source broadening. We interpret this source broadening as a thermal effect and a plot of the equivalent impurity ion temperatures is shown in Fig. 5. In this figure the abscissa is an "equivalent ionisation potential", which for the forbidden metal lines is the ionisation potential of the preceeding ion while for the gases we use the excitation energy from the ground level of the same ion. Notwithstanding the large error bars we note a general increase in the ion temperature with increasing ionisation potential, the "core ions" with temperatures of a few 100 eV being hotter than the peripheral ions. Unfortunately in this series of experiments we have no data during the Alfvén heating pulse with which we can compare these ohmically heated plasma results and this remains a task for a future programme.

VI. ATOMIC STRUCTURE OF 2-ELECTRON SYSTEMS

Following the demonstration by STAMP et al. (1981) on the DITE tokamak that accurate wavelength measurements of the $1s2s\ ^3S - 1s2p\ ^3P$ He-like transitions are feasible in tokamaks, an attempt was made on the TCA tokamak to extend these measurements along the isoelectronic sequence to argon. Since the triplet wavelength scales as Z while relativistic and QED corrections scale as Z^4, with higher order terms, there exists the possibility of making a definitive test of QED theory from precision measurements of the triplet structure for high Z. Unfortunately, the plasma temperature required to observe the He-like 2s-2p, $^3S_1 - {}^3P_0$ line in argon, is close to that required for equal H- and He- like populations, Fig. 1, and this temperature well exceeds that available with the TCA Tokamak. Ion stages as far as Li-like argon were observed. However, data on He-like ions of the lighter gases, neon, oxygen and nitrogen were taken, see eg plate XI, and these represent an improved accuracy on previous measurements. The test gas was added by gas puffing or static filling, without adversely affecting the plasma.

The E766 spectrometer viewed the plasma radially, so that Doppler shifts are expected to be negligible in these spectra. In the plasma conditions pertaining, any plasma rotation would be expected to be small ($v_\phi < 10^6$ cm/sec) and perpendicular to the line of sight of the spectrometer.

A sample of the analysis is shown in Fig. 6 where the $^3P_0 - {}^3P_2$ fine-structure is compared with the best available theory. The data marked "a" represent the present experimental results.

VII. TIME-RESOLUTION OF IMPURITY EMISSION AND CORRELATION WITH OTHER DIAGNOSTICS

Results obtained photographically showed that there is an increase in the intensity of most of the impurity lines when the Alfvén Wave Heating pulse is applied. The general effects of the rf pulse, detailed by DE CHAMBRIER et al. (1982 c) are that the plasma density rises, the electron and ion temperatures increase and the radiated power loss increases. The increased radiated power loss leads to a subsequent electron cooling before the end of the rf pulse. The radiated power profile peaks on axis during the rf pulse as illustrated in Fig. 7. A typical discharge is shown in Fig. 8 in the presence of additional heating, the unheated case being shown as a dotted line.

We studied the ionization states of oxygen and iron accessible to the instrument and typical examples are shown in Fig. 9. It can be seen that there is a rise in the emission from both impurity species, both the light gas and the metallic impurities, during the rf pulse. There is a concommitant increase in electron density during the heating pulse but a large fraction of this increase may be due to the impurity influx itself. We see that the behaviour of the edge lines (O III-O VI) is different to that of the core lines (O VII, Fe XVI, Fe XVIII). The former react quickly at both the start and end of the rf pulse whereas the core ions react more slowly. Also, in the case of the light gas impurities, the emission typically ramps up until the end of the rf heating period whereas the ionised metals, eg Fe XVIII, reach a peak of intensity somewhat later than the temperature peak, and rapidly decrease before the end of the heating pulse. The beha-

viour of the edge lines is reminiscent of the behaviour of the antenna DC potential during the rf pulse, shown in Fig. 10, and may well simply be due to changes in the edge profiles. In Fig. 11 we show a comparison between the line-of-sight-integrated Fe XVIII emission intensity and the line-of-sight-integrated radiated power loss and we see that the temporal behaviours of these two signals are very similar, leading us to the assumption that the radiated power loss increase during the rf pulse is mostly attributable to emission by Fe XVIII and neighbouring iron charge states.

In order to interpret the radiated power profile we modelled the radiated power loss according to the ionisation state equilibrium and reaction rates given by POST et al. (1977). Results are shown in Fig. 12, for various assumptions. Firstly we see that 1 % of iron, with a flat relative concentration has a hollow radial radiated power profile. Adding 3 % of oxygen only serves to increase the radiated power loss at the edge of the plasma. We require an intense peaking of the iron concentration, $N_{Fe}(r)/n_e(r) = (1-r^2/a^2)^4$, to explain the sharp peaking of the radiated power profile during the rf pulse. Again the addition of 3 % of oxygen makes little difference.

A first attempt to model the time dependence of the Fe XVIII emission is shown in Fig. 13. The calculation of the Fe XVIII abundance follows from a time-dependent ionisation code which takes into account the variation of the core density n_e and temperature T_e, and assumes a constant iron impurity concentration. As indicated in the next section, the intensity of the forbidden Fe XVIII line at 974.86Å, "I_{exp}", is rather a good indicator of the Fe XVIII

concentration, being nearly independent of n_e but responsive more to T_e and the ionic concentration. Fig. 13 shows that the calculated Fe XVIII abundance, as expected, follows the variation in T_e quite faithfully in contrast to I_{exp} which is correlated more closely with n_e. Again, a likely interpretation of this is that the time history of the highly-ionised metal is due to an influx into the core of new impurities or an inward accumulation of "old" impurities during Alfven heating and that these impurities themselves are partly responsible for the increase in electron density. The rapid fall-off in the intensity of the highly ionised metal lines before the end of the auxiliary heating pulse must eventually follow the rapid decrease in T_e but there may also be impurity pump-out phenomena during this period of the discharge.

VIII. ABSOLUTE CONCENTRATIONS OF IMPURITIES

In this section we estimate the metallic impurity concentration in the core during the rf pulse by equating the total radiation bolometer signal to the iron line emission. Comparison with the oxygen line emission yields the Fe/O impurity ratio. From the increase in the total radiation and from the intensities of the oxygen and iron lines before and during the rf pulse we can deduce their concentration changes.

In the T_e region 700-900 eV all the metal impurity ions eg, Fe XIX, Fe XVIII, Fe XVII, Cr XVII, Cr XVI, Cr XV, Ni XXI, Ni XX, Ni XIX radiate equitably at about

$$P_{(ion)} = 0.5 \times 10^{-25} \text{ w cm}^{-3} \text{ per free electron per ion} \qquad (1)$$

By inspection of Plates I-VIII we know that iron is the majority impurity, so let us assume that iron is the only metal present as far as the total radiation loss is concerned. We assume coronal balance curves for the core ions. This is a reasonable assumption according to TFR GROUP (1980), even though results on PLT indicate rather lower ionisation 'q' with $\psi_q(r) \propto T_e(r)$ (see also BRETON et al.(1982)). We use Lotz' (ionisation) and Burgess' (recombination) rates (see BRETON et al. (1976)).

$$\begin{aligned} P_{tot}(Fe) &= n_e N(Fe)\, P(Fe) \\ &= n_e^2 \, \frac{N(Fe)}{n_e} \, P(Fe) \end{aligned} \qquad (2)$$

At peak radiated power, $P_{tot} = 2.4$ Wcm^{-3} in the core, at 15 kG, with $\sim$ 90 kW rf power delivered and $n_e(0) = 3.75 \times 10^{13}$ cm^{-3}.

$$\text{i.e. } \frac{N(Fe)}{n_e} = 3.4 \text{ \% in the core} \qquad (3)$$

Together with the strong peaking factor found from the modelling results, this gives $\sim$ 1 % of iron averaged over the total volume of the plasma.

At the measured value of $T_e(0)$ of 850 eV, the most abundant iron ion is Fe XIX (BRETON et al. (1976)). The temperature of maximum Fe XIX abundance quoted in that reference is "a median" between the high value for T_e at Fe XIX maximum abundance quoted by

SUMMERS (1974) and the T_e ($\hat{N}$(Fe XIX) values quoted by other authors, see DRAWIN (1976). A maximum abundance temperature of 850 eV for Fe XIX also seems to be in accord with experimental results on PLT and TFR and is consistent with the most recent results of BRETON et al. (1982). With this assumption we obtain,

$$\frac{Ne(Fe\ XIX)}{N(Fe_{tot})} = 0.2 \text{ at } T_e(0) = 850 \text{ eV} \qquad (4)$$

then,

$$Ne(Fe\ XIX) \simeq 0.2 \times 3.4 \times 10^{-2} \times n_e \qquad (5)$$

$$\simeq 2.4 \times 10^{11} \text{ ions cm}^{-3} \text{ in the core.}$$

This represents a maximum value of the concentration, based on the approximation that all the core metal ions are indeed iron ions.

Fe XIX $2s^2 2p^4\ {}^3P_2 - {}^3P_1$ at 1118.07 Å has a calculated intensity (LAWSON et al. (1981)) given by

$$E\ (1118.07) = 1.37 \times 10^2 \times N(Fe\ XIX)$$

$$= 3.4 \times 10^{13} \text{ph s}^{-1}\text{sr}^{-1}\text{cm}^{-3} \qquad (6)$$

In comparison, the O VI 2s-2p doublet at 1037 Å, 1032 Å, has an intensity

$$I(2s\ {}^2S_{1/2} - 2p\ {}^2P_{3/2,1/2}) \simeq 100 \times I(\text{Fe XIX at } 1118.07\ \text{Å})$$

and since the spectrometer throughout can be considered as constant over this short wavelength range we obtain

$$\frac{I(O\ VI)}{I(Fe\ XIX)} = \frac{L(O\ VI)}{L(Fe\ XIX)} \quad \frac{n_e \langle \sigma v \rangle_{ex}^{2s-2p} \quad N(O\ VI)/4\pi}{E(Fe\ XIX \text{ at } 1118.07\text{Å})} \qquad (7)$$

where 'L' is the plasma depth viewed for each ion.

We plot out in Fig. 13 the ionic distributions with the 'core' ions in quasi-coronal equilibrium, and with the peripheral ions, eg O VI, having inward diffusion velocities $V_z \sim 10^4$ cm/sec. This treatment displaces the O VI peak inwards to a mean radius of $\sim$ 14.5 cm.

$$\begin{aligned} &L(O\ VI) \sim 2x\ 1.5\ cm = 3\ cm, \text{ where } n_e = 1.4 \times 10^{13}, \text{ and } T_e = 85eV. \\ &L(Fe\ XIX) \sim 11\ cm, \text{ centred on the core.} \end{aligned} \qquad (8)$$

$$\langle \sigma v \rangle_{ex}^{2s-2p} = 1.6 \times 10^{-5} \frac{f_{ij}}{\Delta E_{ij}} \bar{g} \exp(-\Delta E_{ij}/kTe),$$

and for O VI, $\bar{g} = 0.9$

$f_{ij} \simeq 0.2$

$\Delta E = 12$ eV

We then obtain

$$\langle \sigma v \rangle_{ex} = \frac{1.4 \times 10^{13} cm^{-3} \times 1.6 \times 10^{-5} \times 0.2 \times 0.9 e^{-12/85}}{12 \times (86)^{1/2}}$$

$$= 3.15 \times 10^5 \ cm^3 \ s^{-1}$$

from which $$n_e \frac{\langle \sigma v \rangle}{4\pi} = 2.51 \times 10^4 \text{ ph sr}^{-1} \text{ s}^{-1} \quad (9)$$

The value of $\bar{g}$ is obtained from COCHRANE and McWHIRTER (1982). We check this value using the formulae given by BRETON et al. (1976),

ie $$\langle \sigma v \rangle_{ex}^{2s-2p} = 10^{-8} \left(\frac{I_H E_1}{(E_0 - E_1) E_0} \right)^{3/2} \frac{q}{2\ell_0 + 1} G(\beta) e^{-\beta}$$

$$= 1.87 \times 10^{-7} \text{ cm}^3 \text{ s}^{-1}$$

by setting $\beta = \frac{\Delta E}{kT}$ and $G(\beta)$ and q as tabulated by BRETON et al.(1976). The O VI 2s - 2p line intensity is then given by

$$n_e \langle \sigma v \rangle_{ex}^{2s-2p} = 1.4 \times 10^{13} \times 1.87 \times 10^{-7}$$

$$\simeq 2.4 \times 10^4 \text{ ph s}^{-1} \text{ sr}^{-1}$$

This value is within a few per cent of the $\bar{g}$ formula, see equation (9).

Using equation (7),

$$\frac{I(1037\text{Å})}{I(1118.07\text{Å})} = \frac{L(\text{O VI})}{L(\text{Fe XIX})} \frac{n_e \langle \sigma v \rangle_{ex}^{2s-2p} N(\text{O VI})/4\pi}{E(\text{Fe XIX at } 1118.07\text{Å})}$$

Inserting experimental values for the left hand side we have

$$\frac{10^2}{1} = \frac{3}{11} \quad \frac{2.5 \times 10^4 \text{ ph sr}^{-1} \text{ s}^{-1} \text{ N(O VI)}}{3.4 \times 10^{13} \text{ ph s}^{-1} \text{ sr}^{-1} \text{ cm}^{-3}}$$

$$\text{ie} \quad \text{N(O VI)} = 5.0 \times 10^{11} \text{ cm}^{-3} \tag{10}$$

$$\frac{\text{N(O VI)}}{n_e(r=14.5)} = \frac{5.0 \times 10^{11}}{1.4 \times 10^{13}}$$

$$\simeq 3.5 \%$$

We note that this again is a maximum, though perhaps a realistic value, based on our "iron only" assumption. In order to compare the concentrations of oxygen and iron we have to relate the peripheral oxygen concentration to that in the core. In many tokamak experiments $N_q(r)/n_e(r)$ is found to be a nearly constant quantity independent of radius and of the charge state q. On this model, then, we find that the ratio of N(Fe)/N(O) is of the order of unity in the core during the Alfven heating pulse.

Turning now to the impurity concentrations before the heating pulse we find in Fig. 7 that the value for P_{rad} (before the rf pulse) $\simeq$ 0.7 W cm^{-3} from the core. We note that even if 4% oxygen were present before the heating pulse, the light gases cannot be responsible for this value of the radiation power loss. Metals therefore must dominate the radiation power loss even before the rf pulse is applied.

The total radiation bolometer signal, Fig. 7, indicates an increase in the radiated power on axis by a factor of between 4 and 6 during the rf pulse. Crudely, we can consider this to be an increase in the product $n_e N(Fe)$. Thus the ratio of the product during the rf pulse to its prior value is then $[\langle n_e\ N(Fe)\rangle]/\langle n_e\ N(Fe)\rangle = 4\text{-}6$. From interferometric data, however, we know that the density increases by about 30 % during the rf pulse. We conclude then that during the rf pulse,

$$\frac{[N(Fe)]}{N(Fe)} \approx 3.7 \qquad (12)$$

Experimentally we observe that the Fe XIX and Fe XVIII line intensities increase typically by between a factor of 2 and 3 at the start of the rf pulse. The temperature increase is not dramatic. It is to be noted, Fig. 15, that the intensities of the forbidden metal lines measured here, in contrast to the OV I lines, have a weaker than linear dependence on n_e. This is because the level populations responsible for the forbidden line intensities are nearly in LTE (see LAWSON et al. (1981)). The intensities of the forbidden lines of Fe XVIII, Fe XIX therefore are good monitors of the iron ion concentrations irrespective of small changes in the plasma parameters.

We may summarize this section with the assertion that the metal-ions with a core concentration of the order of 0.9% n_e are largely responsible for the radiation even before the Alfvén heating pulse and that the rapid rise in radiated power during auxiliary heating is due to a further increase in the metal concentation. This may be the

result of an increased influx of metal impurities or an accumulation on axis of the impurities already in the plasma. In addition we note that the arguments presented here are consistent in the additional sense that if one assumes an oxygen contamination of the order of a few percent of n_e, a typical ungettered tokamak value, then one would deduce, using reverse reasoning, that the volume-averaged iron concentration during Alfvén heating is $\sim$ 1 % of n_e.

IX. SUMMARY

This report is an interim account of collaborative experiments between the CRPP and the Culham Laboratory to investigate the large increase in radiated power associated with the Alfven Wave Heating pulse in the TCA tokamak. Spectroscopic analyses of the radiation in the vacuum ultra-violet region indicate that impurity ions from the component metals of stainless steel are dominantly responsible for the radiation loss. During the rf pulse the concentration of iron in the core can rise to $\sim$ 3 % of the electron density and can radiate away most of the power input from auxiliary heating. An apparent rapid influx and subsequent decay of the metals is observed during the rf pulse. The time-dependence of the radiated power correlates well with the highly-ionised metal radiation from the core and badly with the radiation from low ionization states.

A detailed analysis of the spectral line emission between 3000Å and 250Å is documented in this report and should prove useful for identification purposes in other tokamak experiments.

The wavelength precision of the important diagnostic lines of the ionised metals, chromium, iron and nickel, has been improved. In particular the 3s-3p transitions in Mg- and Na-like ions and the 2s-2p transitions in F- and O-like ions of the metals have been revised. The wavelength resolution of the spectrometer is sufficiently high to deduce ion temperatures in the region 100-400 eV depending on the ion species. The change in ion temperature during the Alfven heating pulse has not yet been measured spectroscopically.

A spectroscopy study of the emission from the rare gases, argon and neon injected into the TCA tokamak has been made in an attempt to measure the Lamb shift contribution to the $1s2s\ ^3S_1 - 1s2p^3P_{2,1,0}$ transition energies in the He-like ions. The electron temperature typically $\sim$ 1 keV was insufficiently high in TCA to produce these transitions in Argon. However improved wavelengths for neon, oxygen, nitrogen and carbon have been deduced and are compared with recent quantum electrodynamic calculations.

ACKNOWLEDGEMENTS

We are grateful to Culham Laboratory for the possibility of using the Normal Incidence Spectrometer on the TCA Tokamak and to H. Jones for his assistance in setting it up at Lausanne. We also thank the other members of the TCA team for their support during this study. The bolometric measurements are the fruit of a collaboration with the University of Fribourg.

The work described was partly supported by the Swiss National Science Foundation.

REFERENCES

BRETON C., DE MICHELIS C. and MATTIOLI M. (1976) EUR-CEA-FC-853.

BRETON C. et al. (1982) EUR-CEA-FC-1159.

DE CHAMBRIER A., CHEETHAM A.D., HEYM A., HOFMANN F., JOYE B., KELLER R., LIETTI A., LISTER J.B. and POCHELON A. (1982 a) Plasma Physics 24, 8, 883.

DE CHAMBRIER A., CHEETHAM A.D., HEYM A., HOFMANN F., JOYE B., KELLER R., LIETTI A., LISTER J.B., POCHELON A., SIMM W., TONINATO J.L. and TUSZEL A. (1982 b) Proceedings of the 3rd Joint Varenna-Grenoble International Symposium Vol. I, 161 EUR7979EN.

DE CHAMBRIER A., CHEETHAM A.D., HEYM A., HOFMANN F., JOYE B., KELLER R., LIETTI A., LISTER J.B., POCHELON A., SIMM W., TONINATO J.L. and TUSZEL A. (1982 c) Proceedings of the 9th International Conference on Plasma Physics and Controlled Nuclear Fusion Research, Baltimore (USA).

DE CHAMBRIER A., HEYM A., HOFMANN F., JOYE B., KELLER R., LIETTI A., LISTER J.B., MORGAN P.D., PEACOCK N.J., POCHELON A. and STAMP M.F. (1982 d) Lausanne Report LRP 216/82.

CHEETHAM A.D., HEYM A., HOFMANN F., HRUSKA K., KELLER R., LIETTI A., LISTER J.B., POCHELON A., RIPPER H., SCHREIBER R. and SIMIK A. (1980 a) Lausanne Report LRP 162/80.

CHEETHAM A.D., HEYM A., HOFMANN F., HRUSKA K., KELLER R., LIETTI A., LISTER J.B., POCHELON A., RIPPER H., SIMIK A. and TUSZEL A. (1980 b) 11th Symp. on Fusion Technology, Oxford, Vol. 1, 601.

COCHRANE D.M. and MCWHIRTER R.W.P. (1982) Rutherford Appleton Report RL 82-099.

DRAWIN H.W., Eur-CEA-FC-858 (1976)

ELDEN B. (1982) Physica Scripta 26, 71-83.

FAWCETT B. (1970) J. Phys. B3, 1152.

HINNOV E. (1979) J. Phys. 230 L197.

KAUFMANN V. and ELDEN B. (1974) J. Phys. Chem. Ref. Data 3, 825.

LAWSON J.D. , PEACOCK N.J. and STAMP M.F. (1981) J. Phys. B14, 1929-1952.

POST D.E., JENSEN R.V., TARTER C.B., GRASBERGER W.H. and LOKKE W.A. (1977) Atomic Data and Nuclear Data Tables 20, 5, 397.

STAMP M.F., ARMOUR I.A., PEACOCK N.J. and SILVER J.D. (1981) J. Phys. B14, 3551-61.

SUMMERS H.P., Appleton Laboratory Report IM 367 (1974)

TFR GROUP (1980) EUR-CEA-FC-1033

WIDING K.G. and PURCELL J.D. (1976) Ap. J. 20 L151.

PLATE CAPTIONS

Plate I VUV Spectrum 280- 635 Å

Plate II VUV Spectrum 580- 990 Å

Plate III VUV Spectrum 950-1150 Å

Plate IV VUV Spectrum 1100-1300 Å

Plate V VUV Spectrum 1300-1500 Å

Plate VI VUV Spectrum 1510-1680 Å

Plate VII VUV Spectrum 1800-2080 Å

Plate VIII VUV Spectrum 2270-2740 Å

Plate IX VUV Spectrum 1200-1350 Å, Neon-doped

Plate X VUV Spectrum 1550-1700 Å, Neon-doped

Plate XI VUV Spectrum 1230-1300 Å, comparison between spectra with and without Neon-doping.

TABLE 1

FILM No.	WAVELENGTH RANGE	SHOTS SERIES (TOTAL)	q_a(min)	$n_e(10^{13}/cm^3)$	NOTES
1)	1300 - 1700	7606 - 7609 (3)	7.0	2.4	A F G H I
2 a)	2300 - 2700	7613 - 7615 (3)	4.5	2.3	A F Sp H I
b)	2300 - 2700	7616 - 7618 (3)	4.5	2.5	A F Sp H I
3 a)	2300 - 2700	7621 - 7628 (8)	4.5	2.4	A F H I
b)	2000 - 2400	7629 - 7631 (3)	5.0	1.9	A F H I
4 a)	800 - 1200	7657 - 7659 (3)	6.0	1.5	A F H I
b)	1450 - 1850	7660 - 7662 (3)	6.0	1.8	A F H I
5 a)	400 - 800	7677 - 7681 (5)	5.0	1.8	A F H I
b)	1000 - 1400	7682 - 7684 (3)	5.0	1.6	A F H I
6 a)	250 - 650	7715 - 7725 (10)	5.5	2.0	B F H I
b)	400 - 800	7726 - 7730 (5)	5.0	2.3	B F H I
7)	210 - 610	7753 - 7763 (10)	4.5	2.7	B F H I
8)	600 - 1000	7768 - 7774 (7)	4.5	2.2	B F I
9)	300 - 700	7775 - 7780 (6)	5.0	2.4	B F I H
10)	300 - 700	7784 - 7789 (6)	5.0	2.5	B F Sc5 H
11)	400 - 800	8155 - 8125 (11)	4.5	2.9	B F Ar Sc5

FILM No.	WAVELENGTH RANGE	SHOTS SERIES (TOTAL)	q_a(min)	$n_e(10^{13}/cm^3)$	NOTES
12 a)	400 - 800	8172 - 8174 (3)	4.8	1.5	B F Ar Sc5 Sh
b)	400 - 800	8175 - 8184 (10)	4.5	1.7	B F Ar Sc5 Sh
13)	400 - 800	8185 - 8200 (15)	4.8	1.5	B F Ar I Sh
14 a)	650 - 850	8204 - 8207 (4)	3.8	2.2	C F Ar I Sh
b)	750 - 950	8208 - 8213 (6)	4.0	2.1	C F Ar I Sh
15 a)	950 - 1150	8214 - 8219 (6)	4.0	1.8	C F Ar I Sh
b)	1170 - 1370	8220 - 8225 (6)	4.0	2.1	C F Ar I Sh
16)	505 - 705	8235 - 8237 (3)	4.6	1.8	C F Ar Sc5 Sh
17)	1170 - 1370	8238 - 8291 (48)	4.0	1.8	C F Ar I Sh
18 a)	1260 - 1460	8294 - 8299 (6)	4.3	1.5	C F Ar R I Sh
b)	1040 - 1240	8300 - 8305 (6)	4.2	1.6	C F Ar R I Sh
19)	1150 - 1350	8308 - 8311 (4)	4.2	1.7	C F Ne I Sh
20)	1100 - 1300	8313 - 8326 (13)	4.2	2.0	C F Ne Sc5 Sh
21)	1215 - 1415	8339 - 8348 (10)	4.2	2.4	C M Ne I Sh
22)	1160 - 1360	8350 - 8379 (30)	3.7	2.2	C M Ne I Sh
23)	1160 - 1360	8380 - 8396 (15)	4.3	2.7	C M Ne Sc5 Sh
b)	1490 - 1690	8397 - 8403 (7)	3.8	2.3	C M Ne N I Sh
24 a)	1490 - 1690	8407 - 8411 (5)	4.5	2.2	C M Ne N I Sh

FILM No.	WAVELENGTH RANGE	SHOTS SERIES (TOTAL)	q_a(min)	$n_e(10^{13}/cm^3)$	NOTES
24 b)	1490 - 1690	8412 - 8414 (3)	4.4	2.3	C M N I Sh
25)	400 - 800	8172 - 8174 (6)	4.8	1.5	A M I Sh
26 a)	1700 - 2100	8424 - 8426 (3)	4.3	2.1	A M N I Sh
b)	1700 - 2100	8427 - 8432 (6)	4.3	1.9	A M N I Sh
27 a)	1480 - 1680	8439 (1)	3.8	1.6	C M N Sh I
b)	1480 - 1680	8440 - 8446 (7)	3.9	1.6	C M Ne Sh I
28)	1160 - 1360	8449 - 8476 (28)	3.8	2.4	C M Ne Sh I
29 a)	1300 - 1500	8594 - 9603 (10)	3.7	2.1	C M I Sh
b)	1100 - 1300	8604 - 8613 (10)	3.9	1.9	C M I Sh
30)	670 - 870	8650 - 8658 (9)	3.8	1.8	C M Sh I
31 a)	950 - 1150	8659 - 8663 (6)	4.0	1.6	C M I Sh
b)	1500 - 1700	8664 - 8672 (9)	3.8	1.8	C M I Sh
32)	1300 - 1500	8673 - 8683 (15)	3.8	1.8	C M I Sh
33)	1300 - 1700	8723 - 8732 (9)	3.6	2.1	A F I Sh
34)	2000 - 2400	8733 - 8745 (12)	3.6	2.1	A F I Sh

Notes:
A λ(Blaze)=1500Å(1200 l/mm)
B λ(Blaze)= 450Å(1200 l/mm)
C λ(Blaze)=1350Å(2400 l/mm)
Sh Shuttered
H With RF

S_p Spectrosil window
F 15.1 kG
M 11.6 kG
L 7.8 kG
Sc5 Sc5 Film

Ar + Argon
Ne + Neon
N + Air
I 101 Film
R Runaway

G Graphite Limiter

TCA TOKAMAK

VUV SPECTRUM

280-635Å

PLATE 1

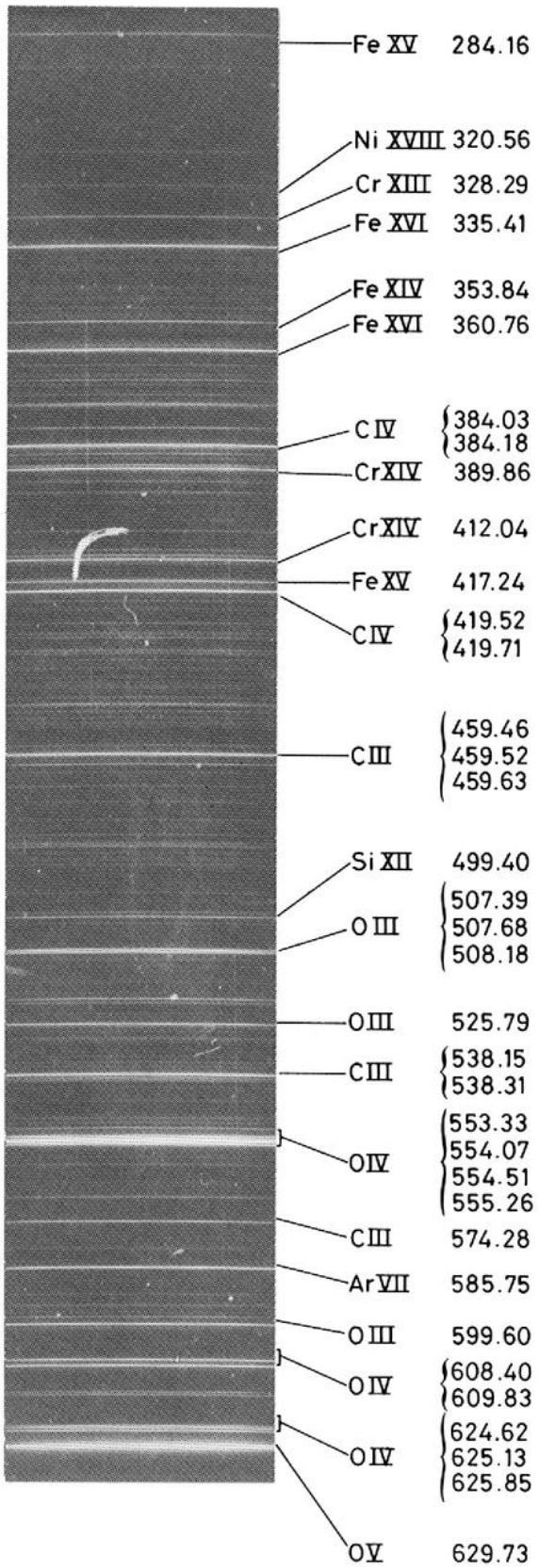

TCA TOKAMAK
VUV SPECTRUM
580 - 990 Å

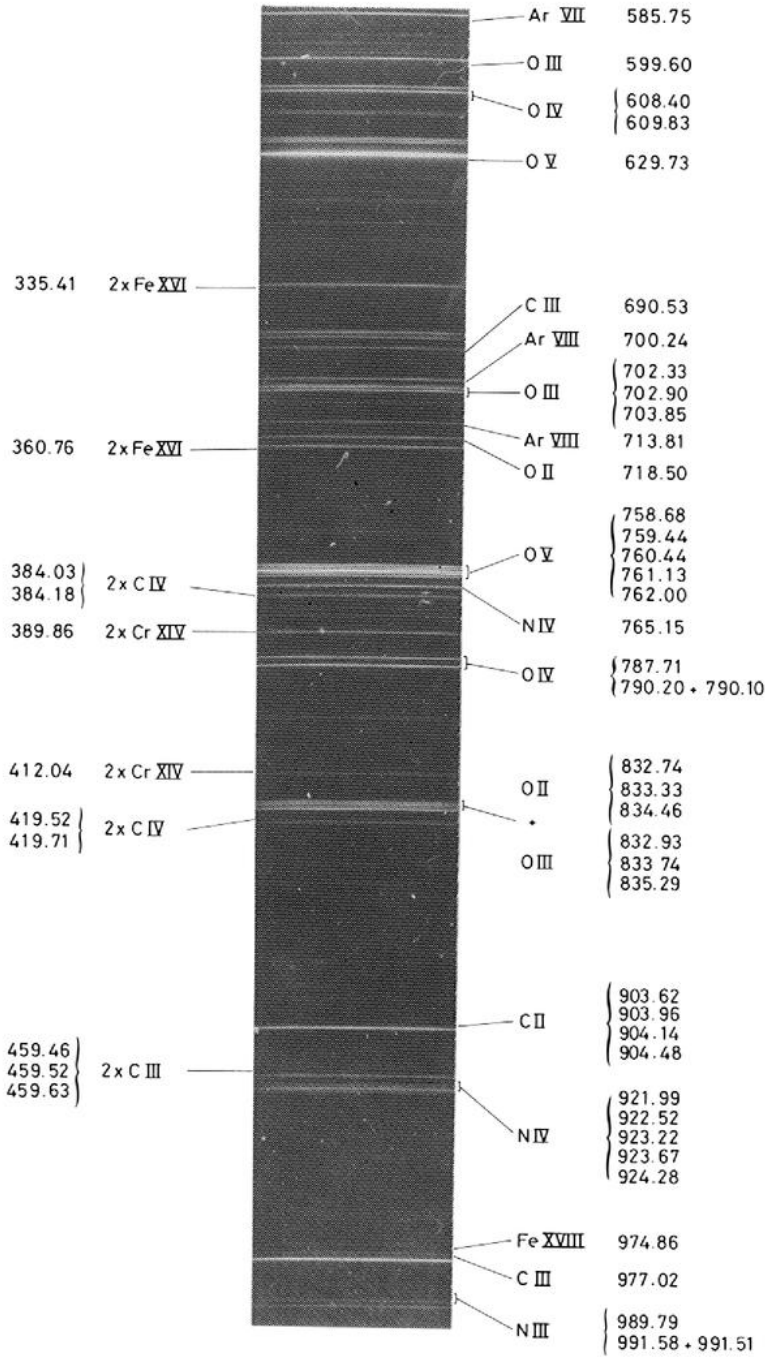

TCA TOKAMAK

PLATE III

VUV SPECTRUM

950 - 1150Å

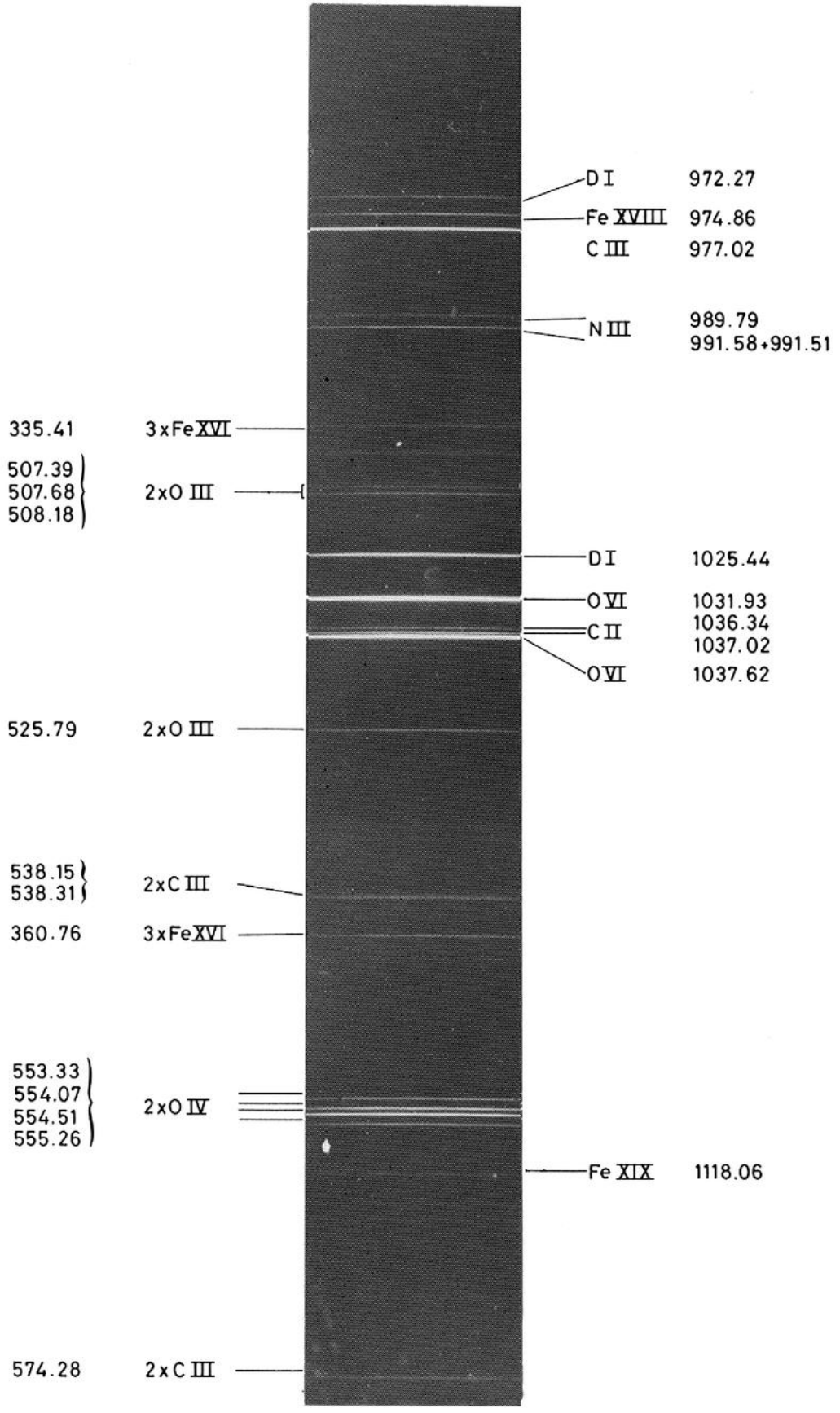

TCA TOKAMAK

VUV SPECTRUM

1100 - 1300 Å

PLATE IV

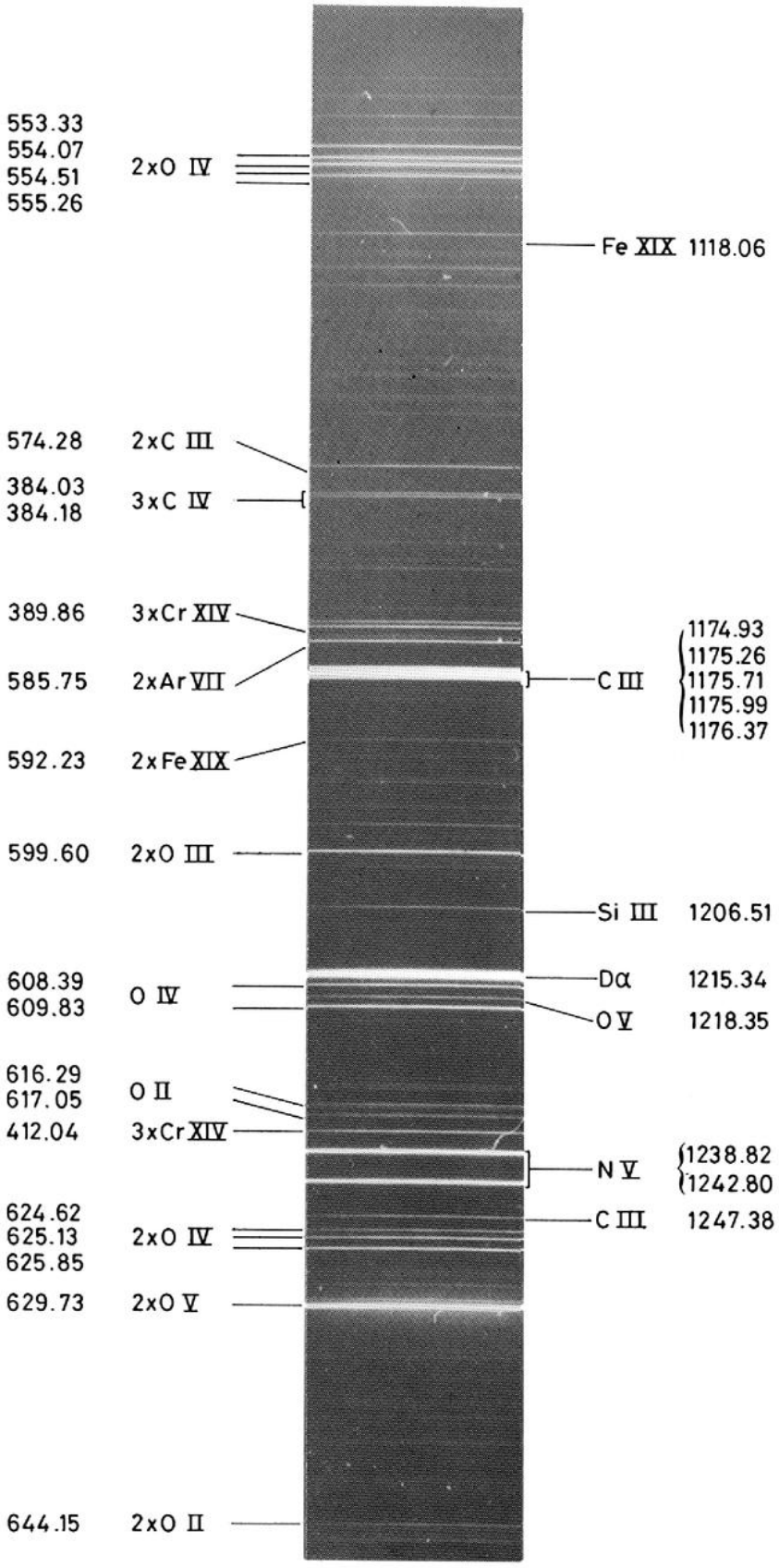

TCA TOKAMAK

PLATE V

VUV SPECTRUM

1300 - 1500Å

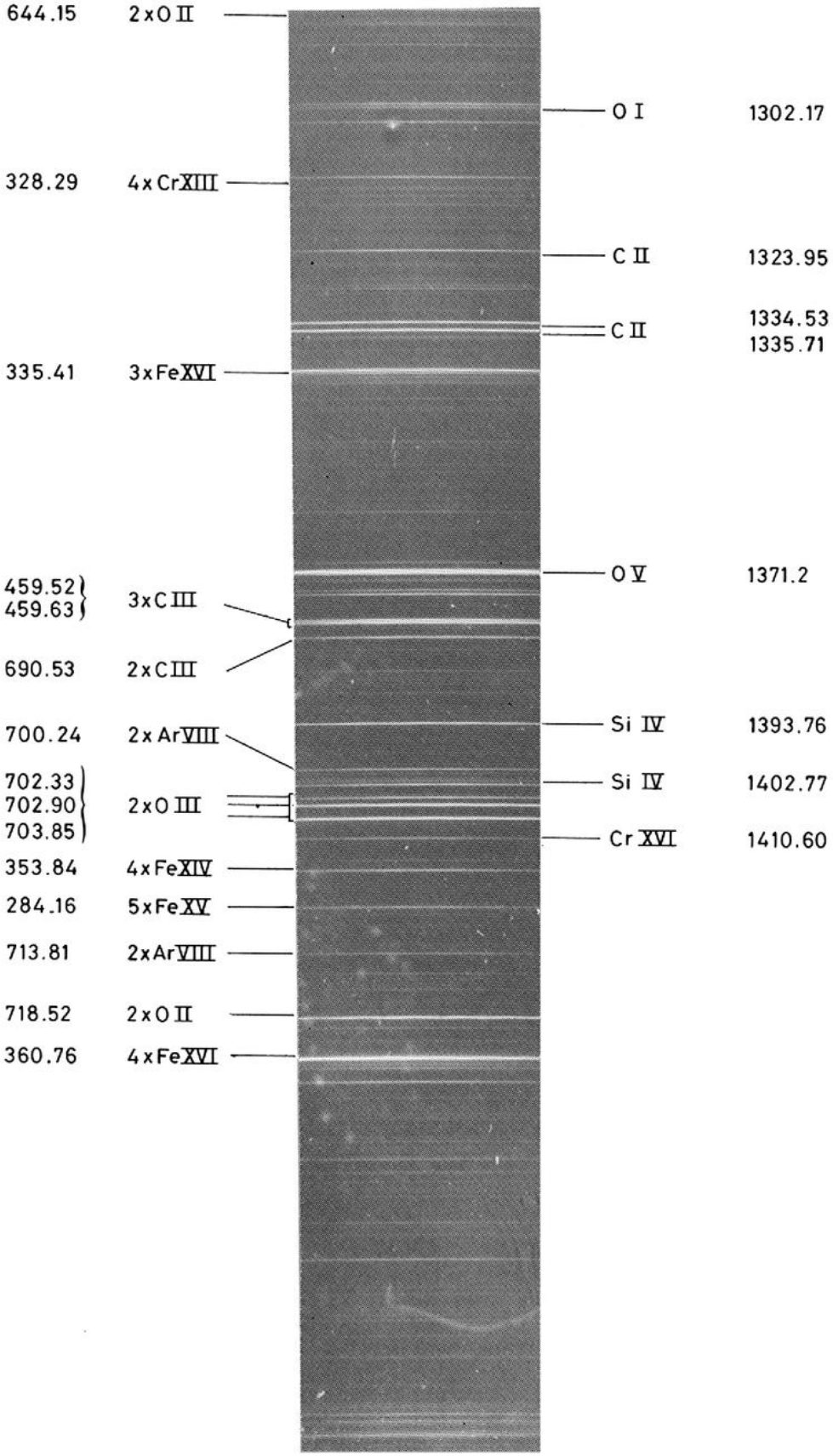

TCA TOKAMAK

VUV SPECTRUM

1510 - 1680Å

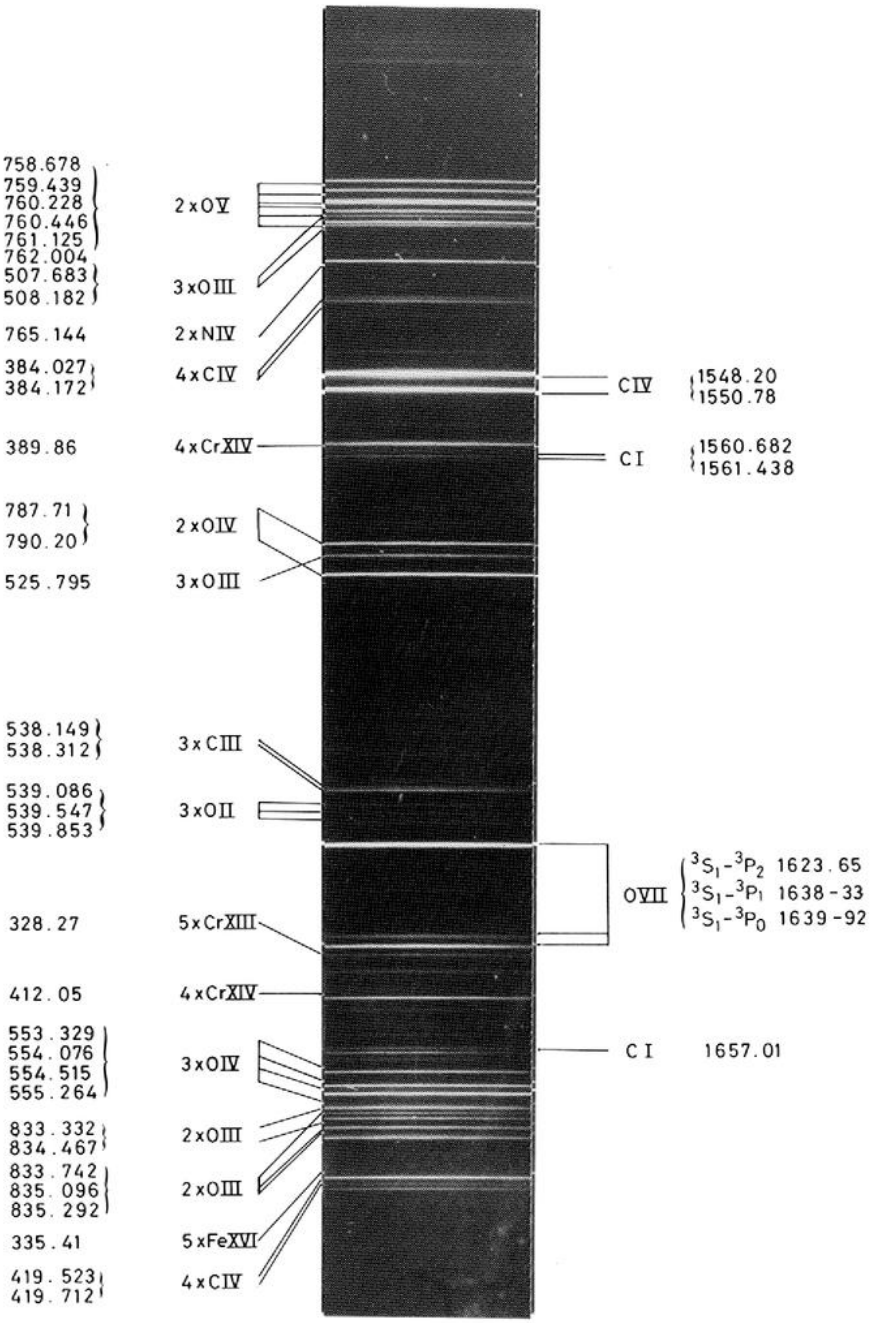

TCA TOKAMAK

VUV SPECTRUM

1800-2080Å

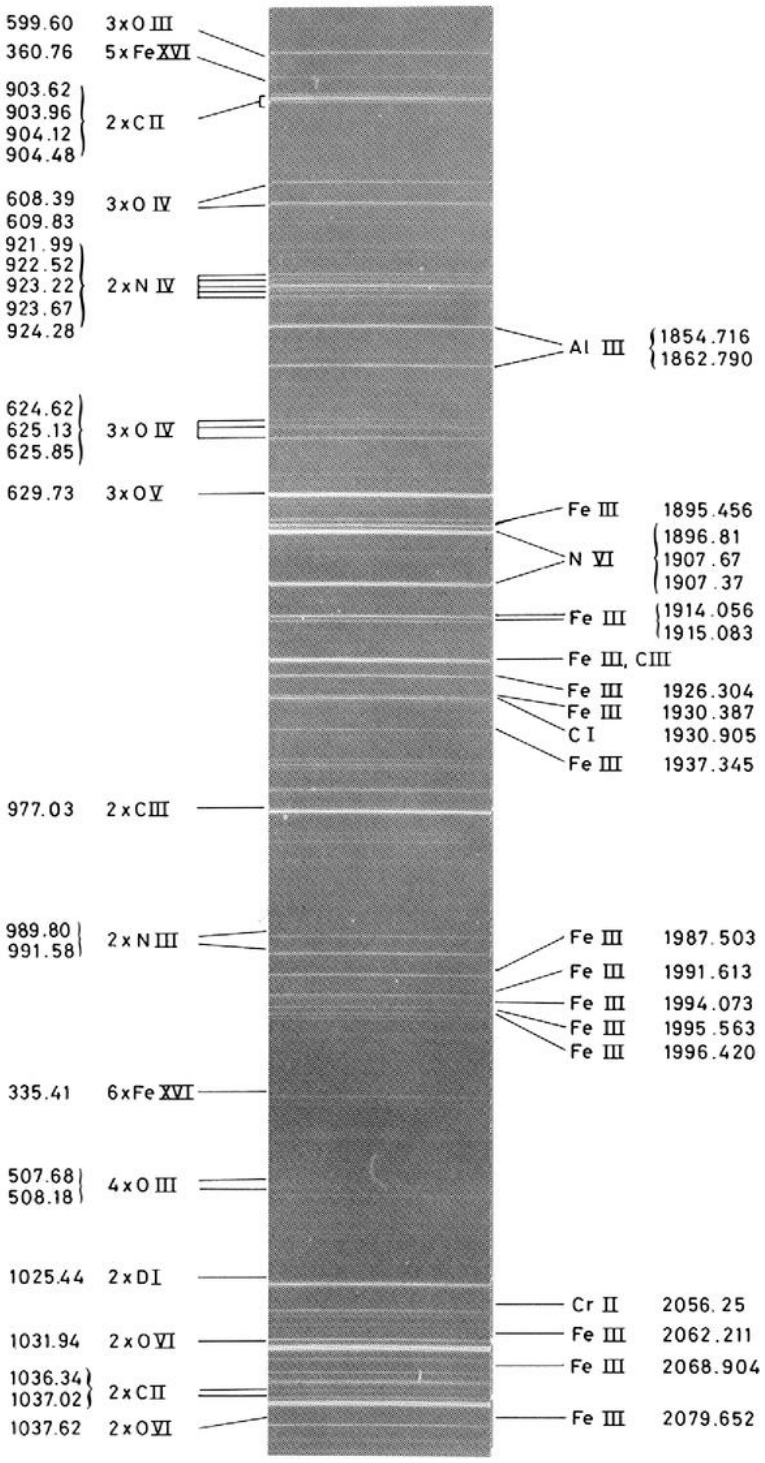

TCA TOKAMAK

UV SPECTRUM

2270 - 2740Å

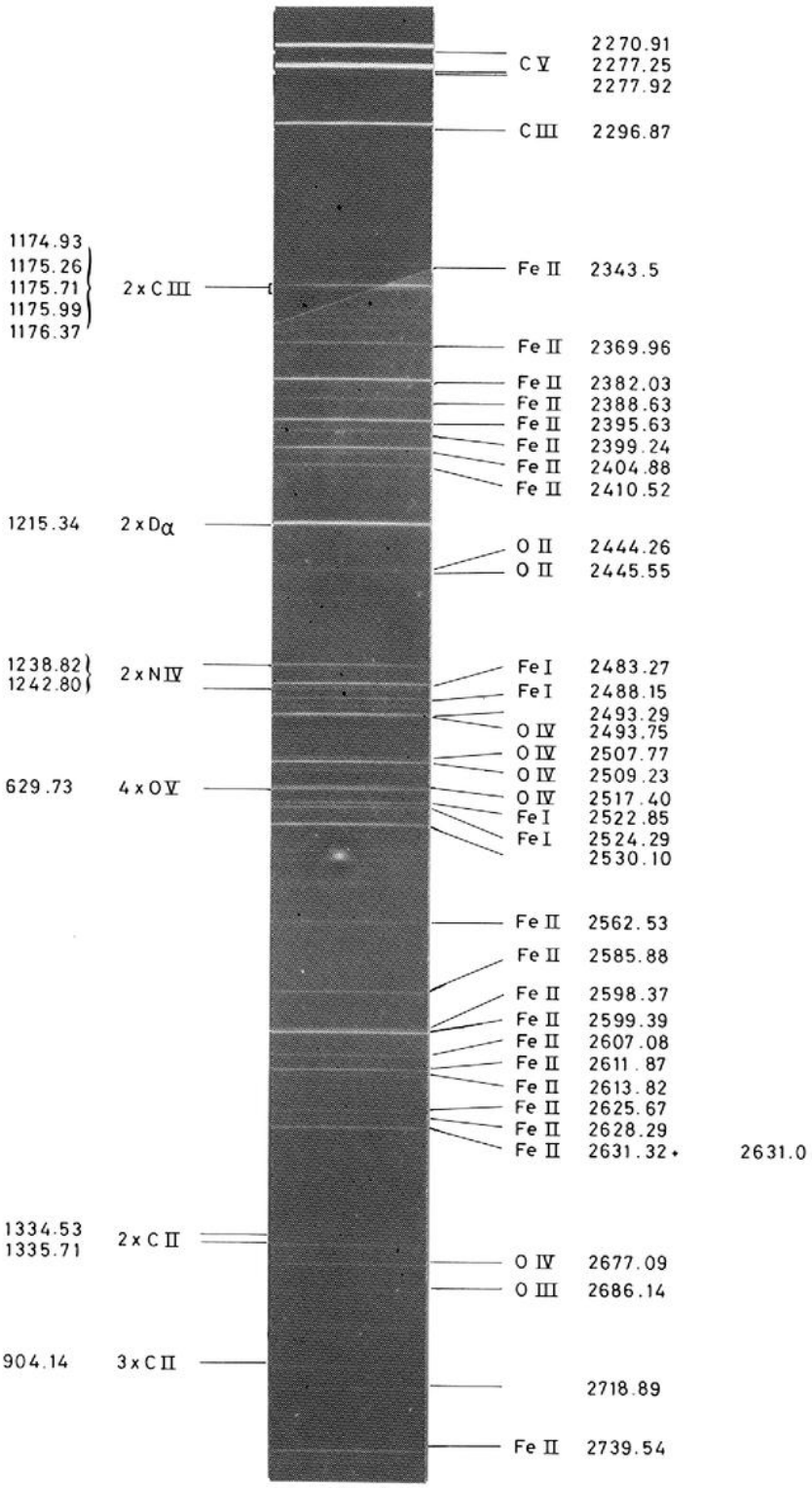

TCA TOKAMAK

WITH NEON IMPURITY INJECTION

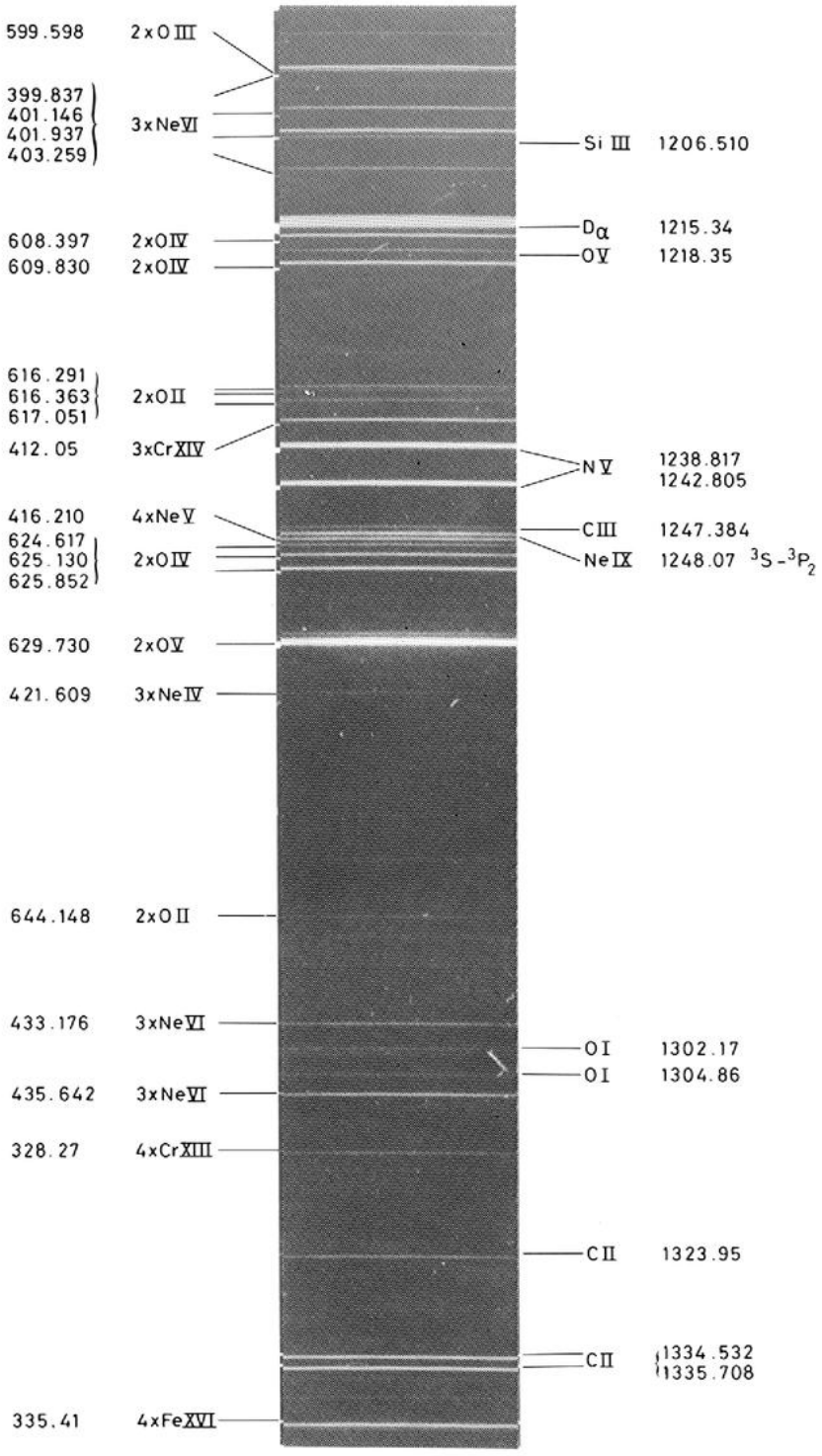

TCA TOKAMAK

VUV SPECTRUM

WITH NEON IMPURITY INJECTION

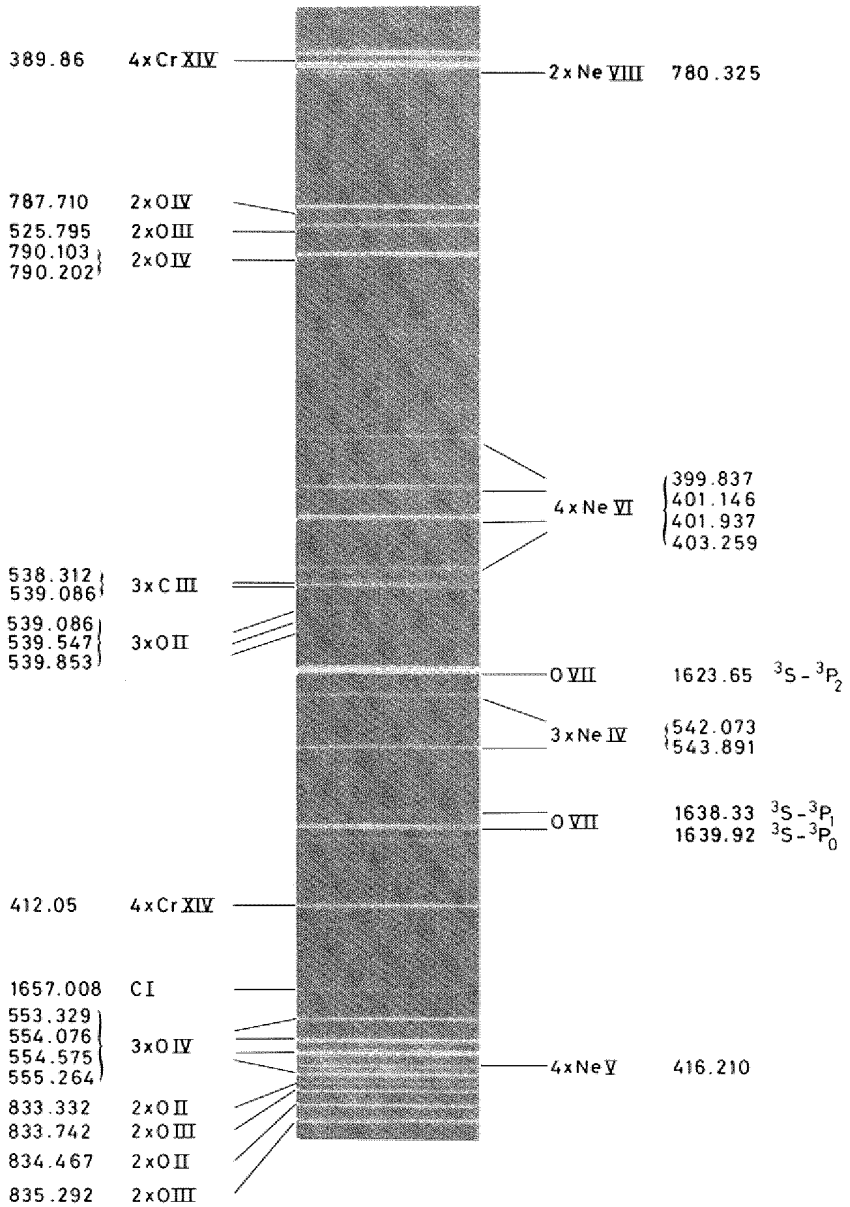

TCA TOKAMAK VUV SPECTRUM
1230 - 1300 Å

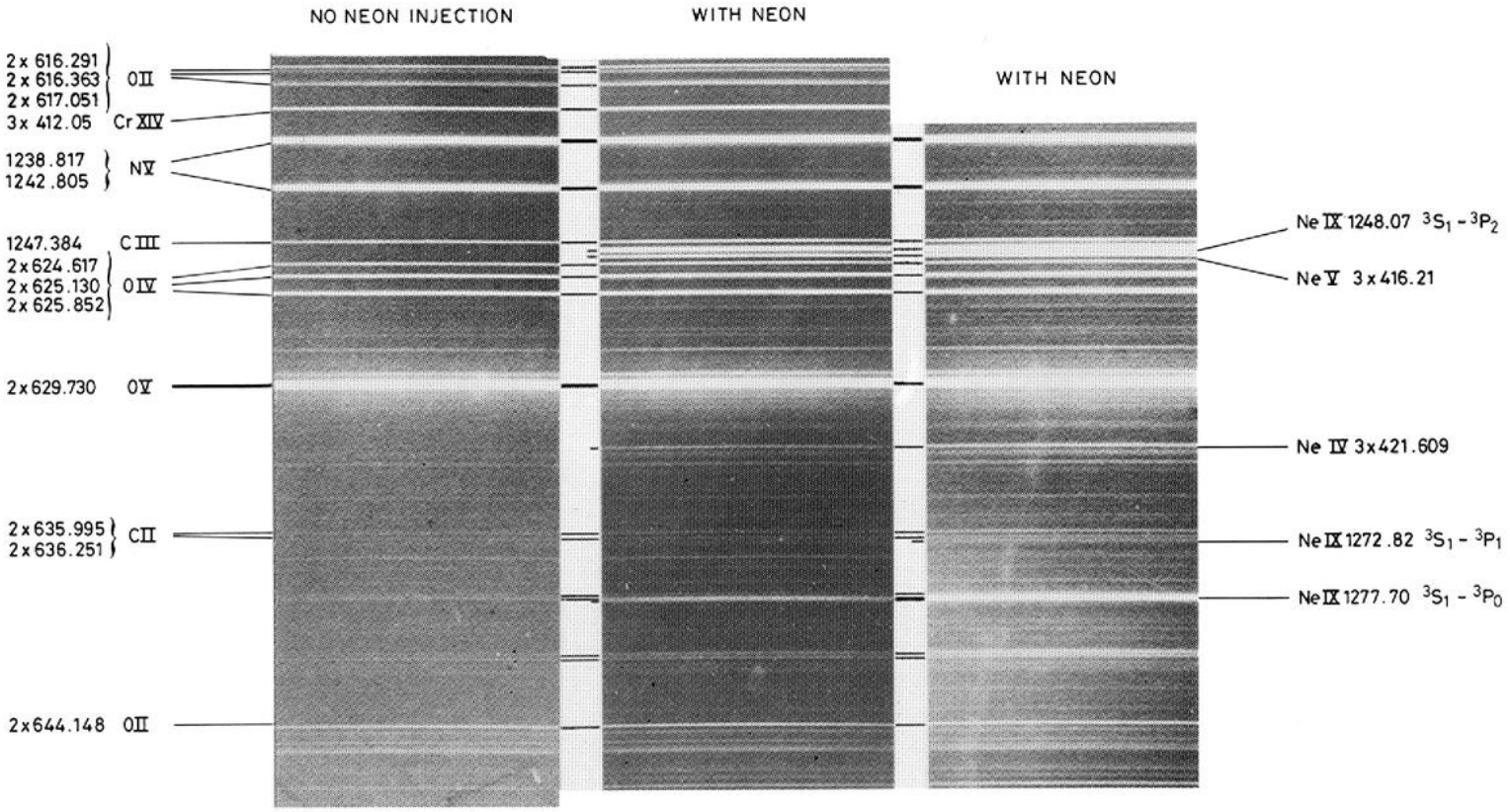

SPECTROMETER SLIT WIDTH =	0.030 mm	0.025 mm	0.045 mm
EXPOSURE TIME =	0.7 s	1.8 s	1.8 s

PLATE XI

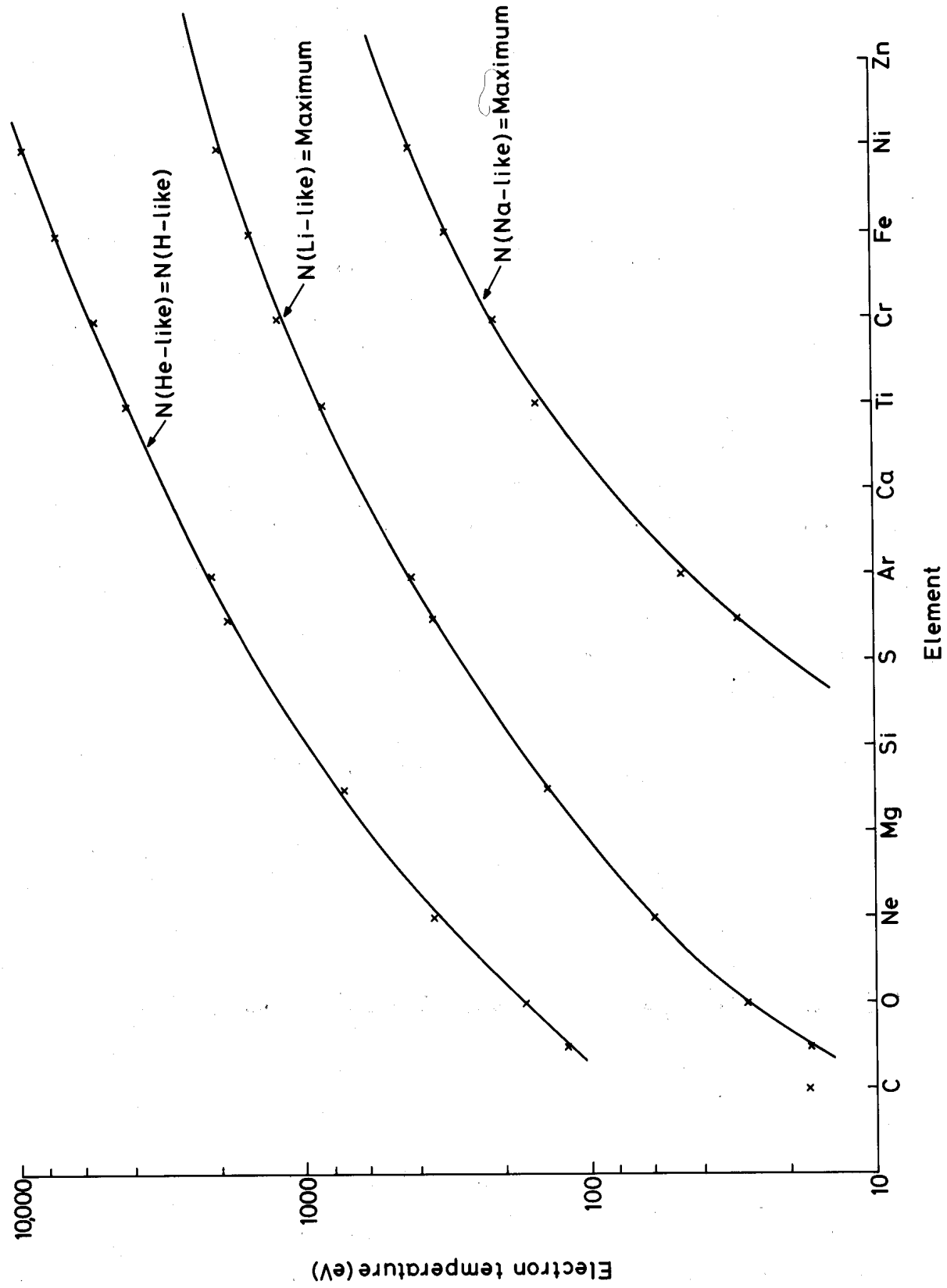

Fig. 1 Electron temperatures at which a)Lithium-like states dominate, b) Sodium-like states dominate and c) Hydroqen-like and Helium-like ionization states are equally probable.

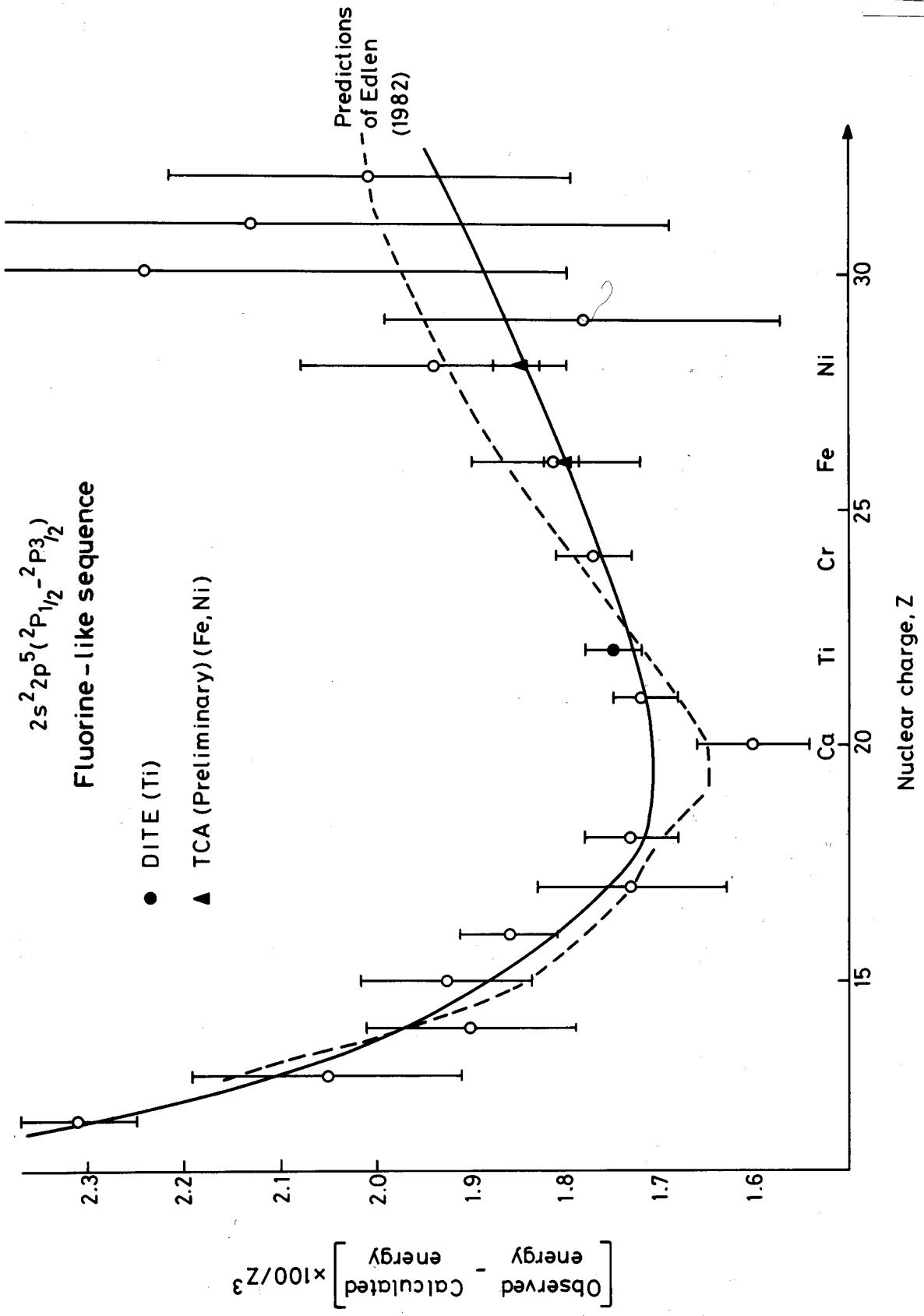

Fig. 2 Comparison between experimental data and the Edlen (1982) prediction for the Fluorine-like transition $2s^2 2p^5 (^2P_{1/2} - ^2P_{3/2})$.

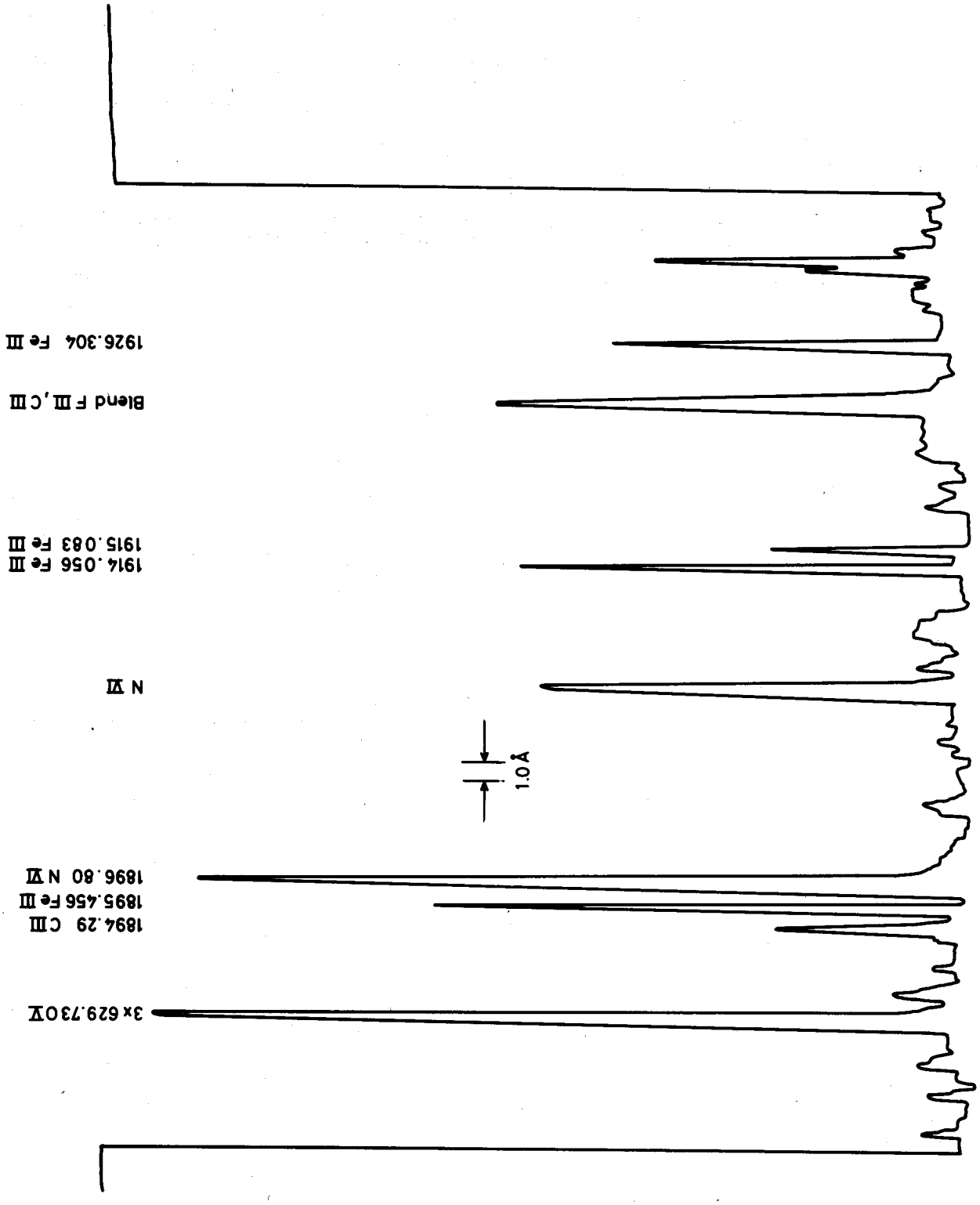

Fig. 3 Densitogram of a photographic plate showing impurity lines in the range 1885Å-1930Å.

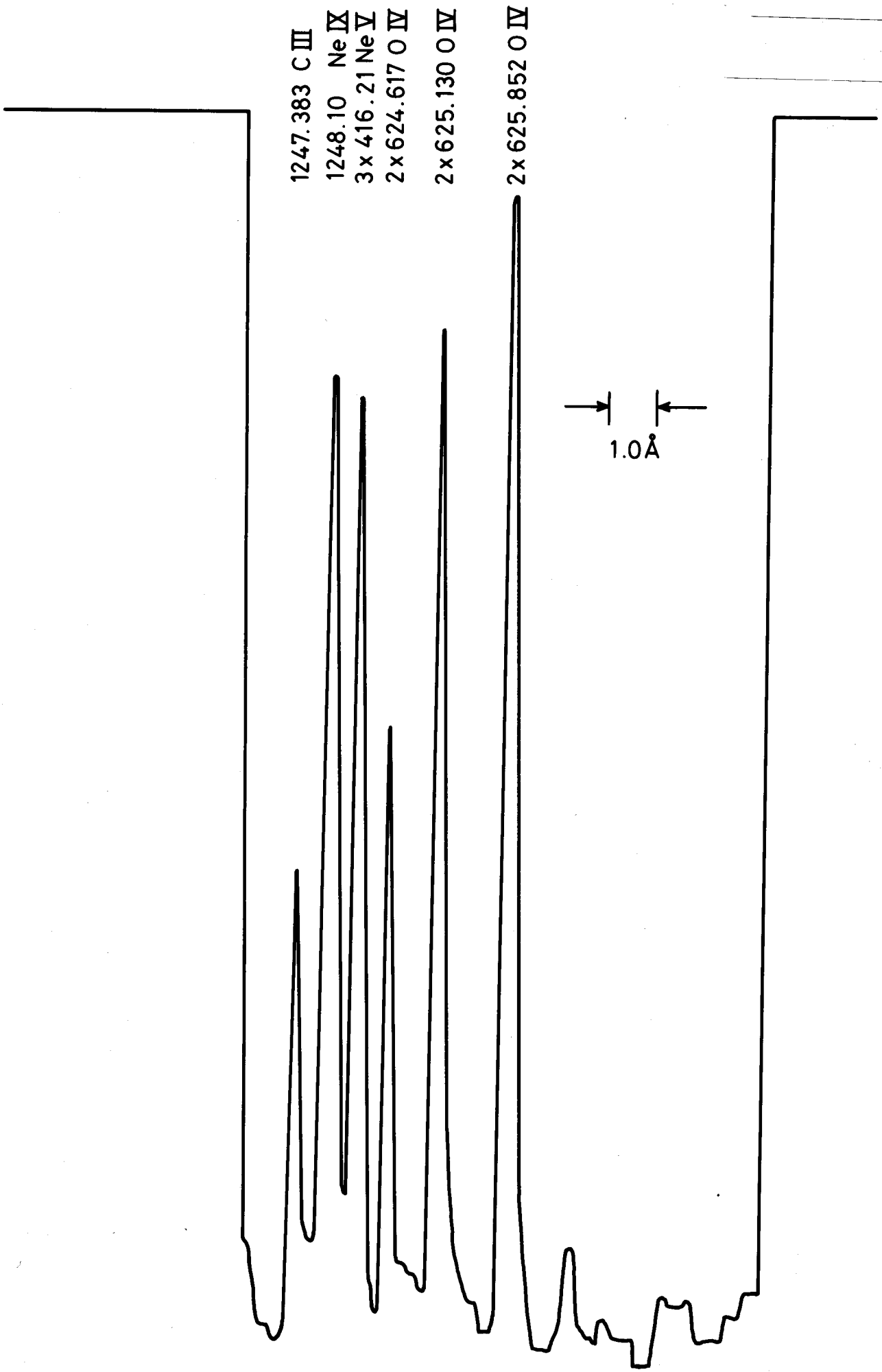

Fig. 4 Densitogram of a photographic plate showing impurity lines in the range 1246Å - 1255Å.

Fig. 5 Ion temperature of the impurity ion states measured from the Doppler width, as a function of the ionization potential of that particular ion state.

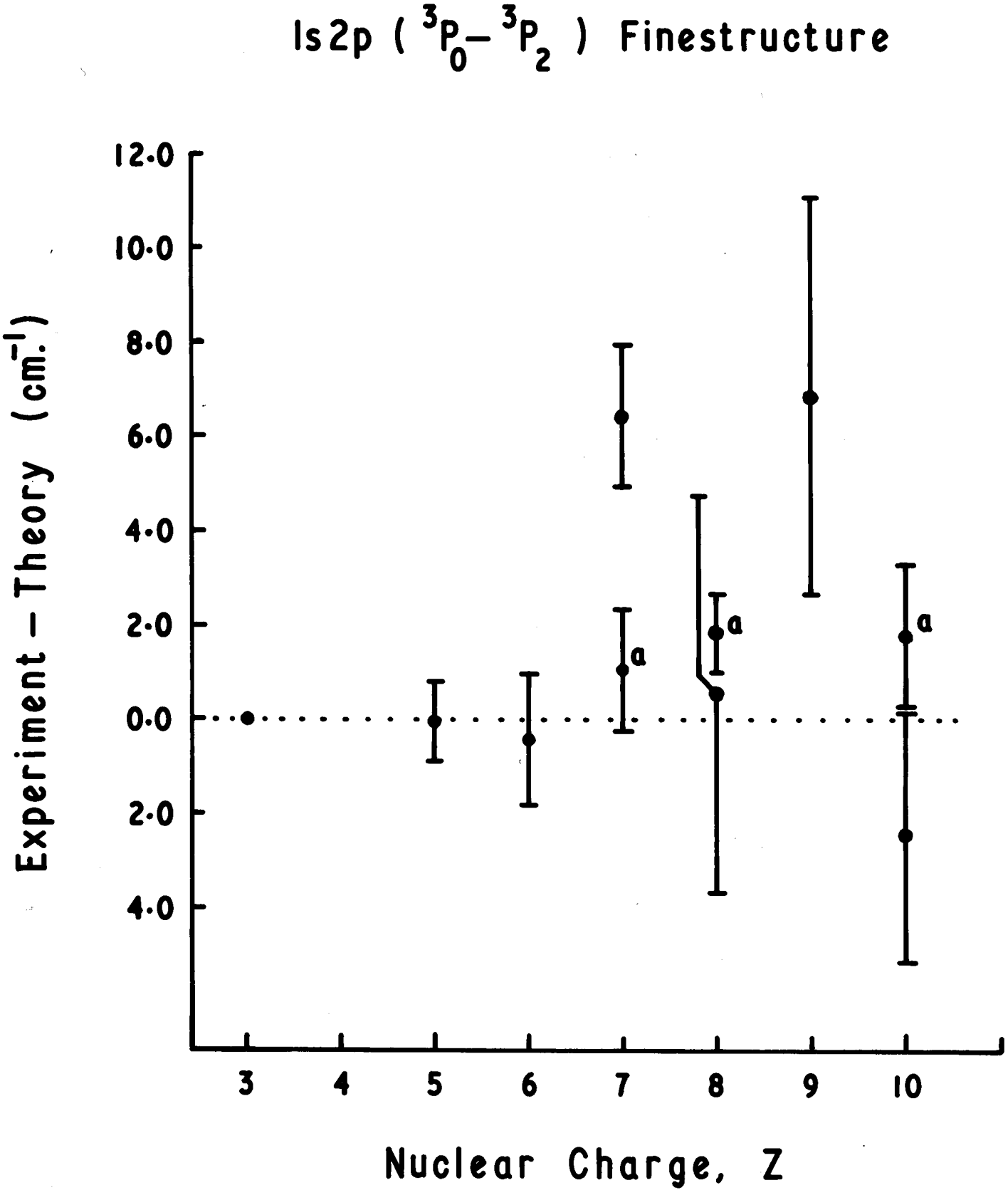

Fig. 6 Fine-structure of the transition 1s2p($^3P_0 - ^3P_2$) for various nuclear charges, compared with the theoretical predictions.

Fig. 7 Radial profile of the radiated power loss during the rf pulse. [15.2 kG, D_2, q=4.5].

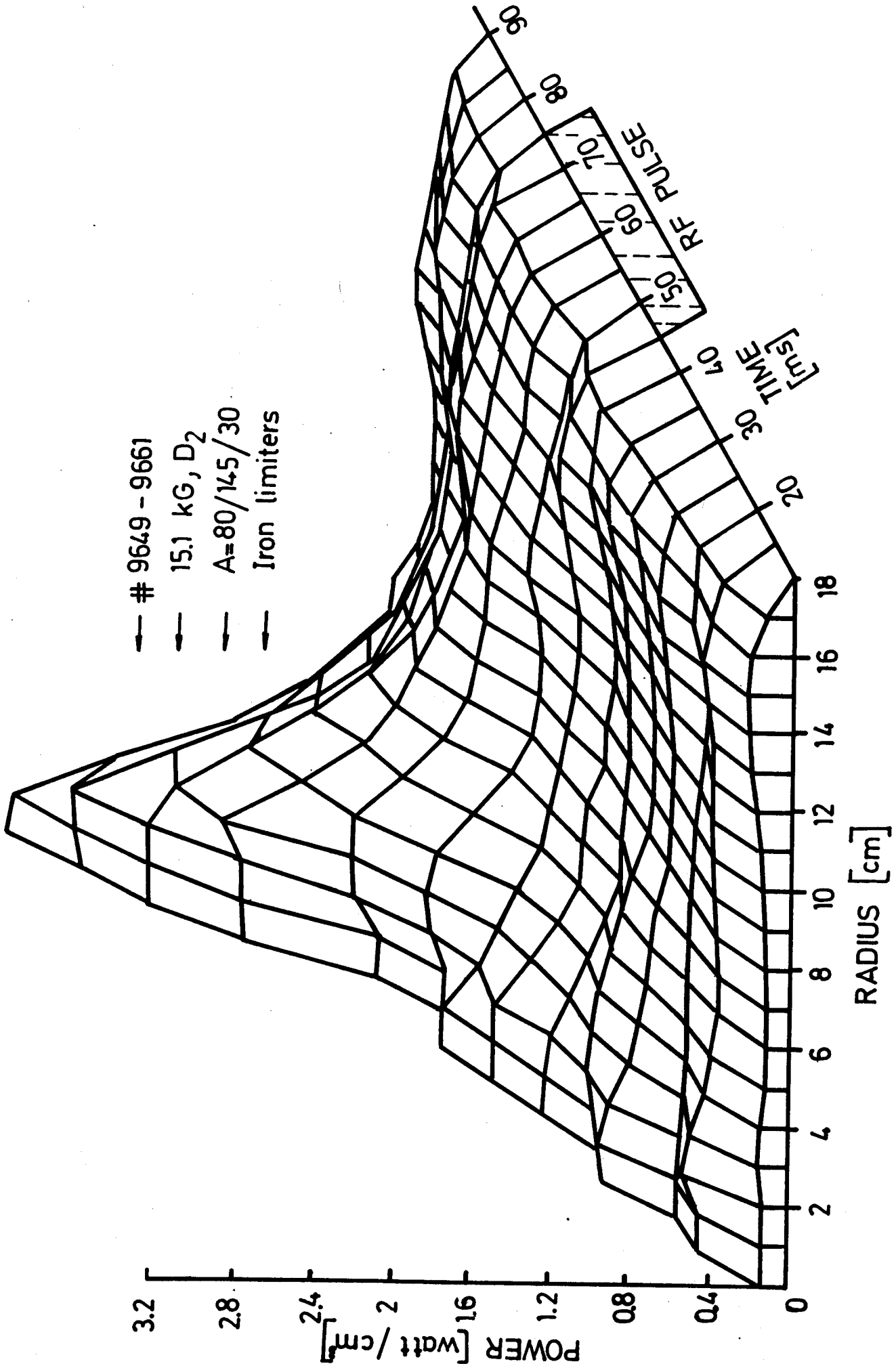

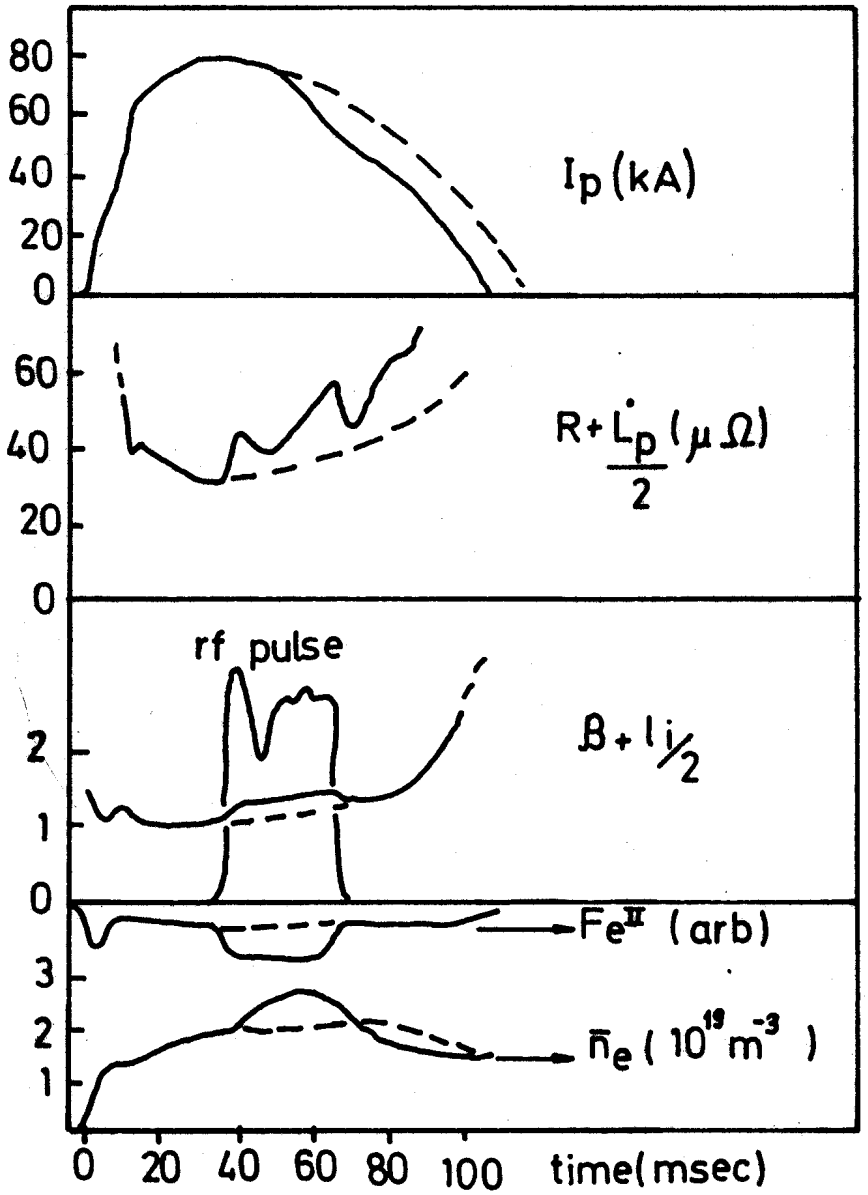

Fig. 8 Effects of the rf pulse on the main plasma discharge characteristics. The unheated condition is shown as dotted lines [15 kG, D_2].

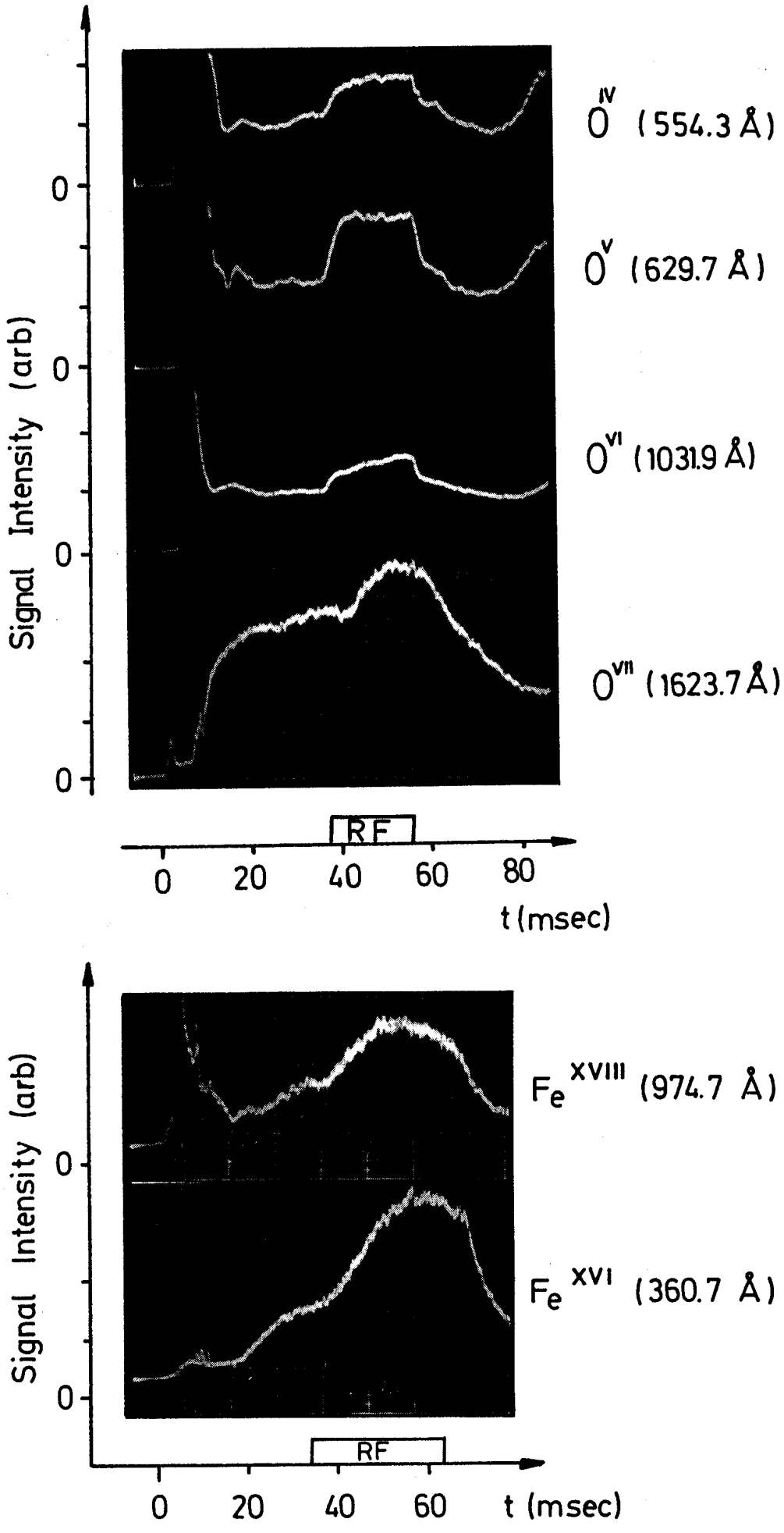

Fig. 9 Time-dependence of impurity lines of a) oxygen and b) iron [15 kG, D_2].

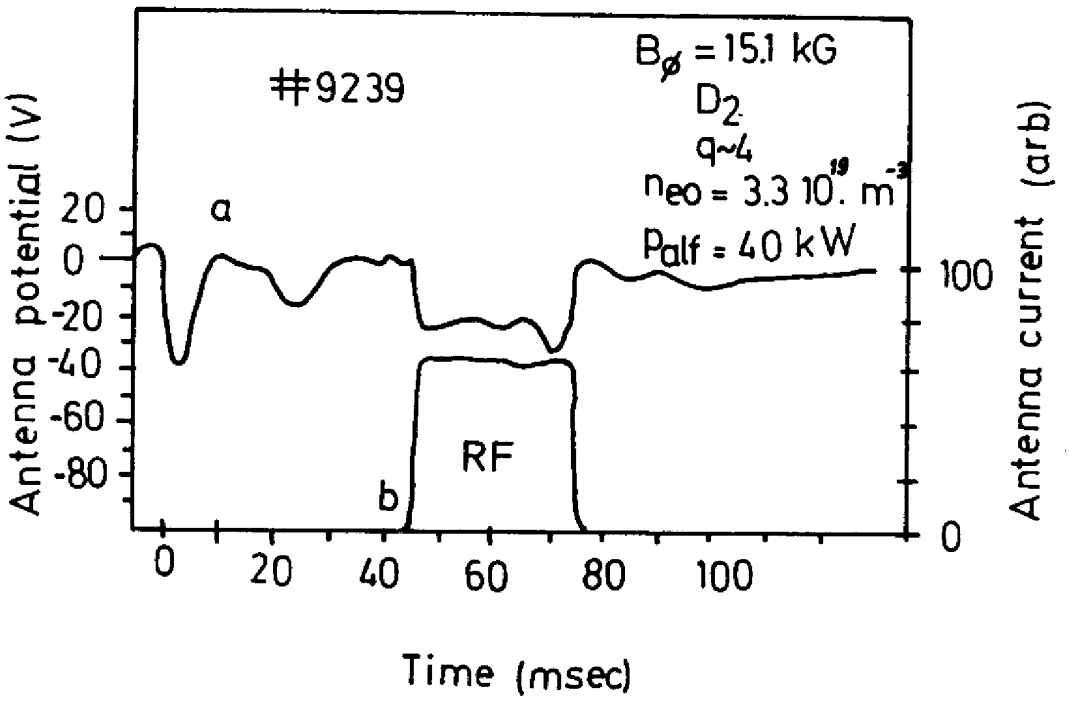

Fig. 10 Time dependence of the antenna DC potential during the rf pulse.

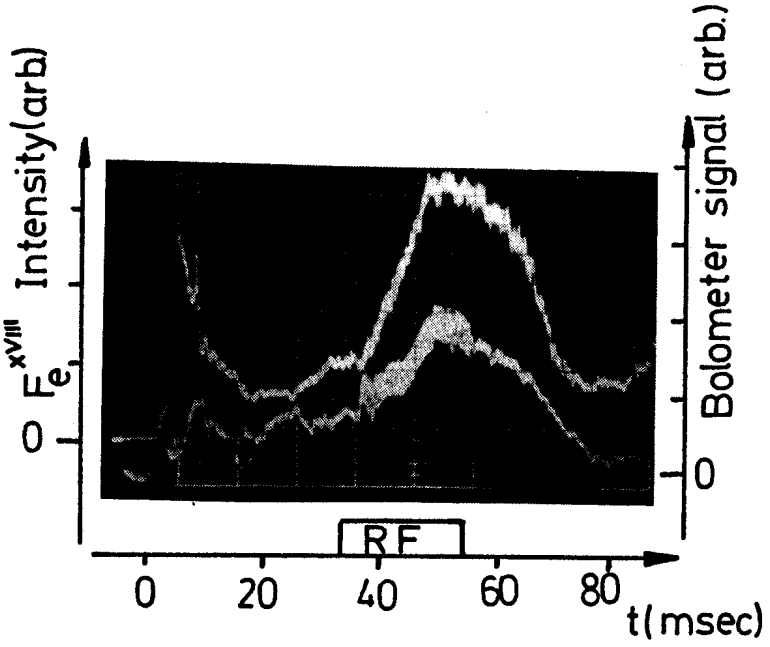

Fig. 11 Comparison between line-of-sight-integrated total radiated power and line-of-sight-integrated Fe XVIII (974.9Å) emission intensity as a function of time.

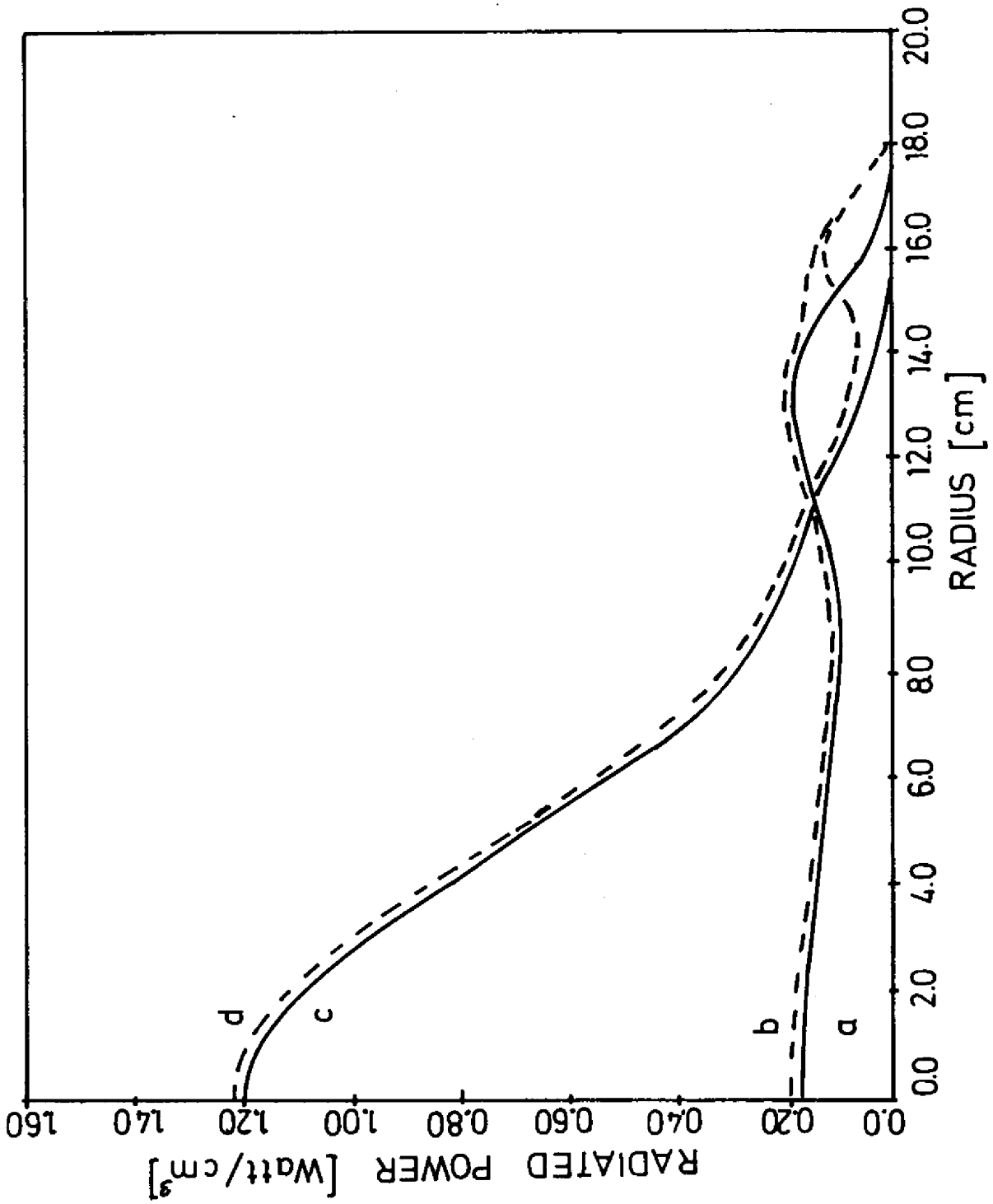

Fig. 12 Modelled radiated power profile on the assumptions

a) 1 % Iron only, $n_e = (1-r^2/a^2)$, $Fe(r) \sim n_e e(r)$

b) Iron as in a), with 3 % oxygen $n_{ox}(r) \sim ne(r)$

c) 1 % Iron only, $n_{Fe}(r) \sim ne(r)\ (1-r^2/a^2)^4$

d) Iron as in c), with 3 % oxygen $n_{ox}(r) \sim n_e(r)$

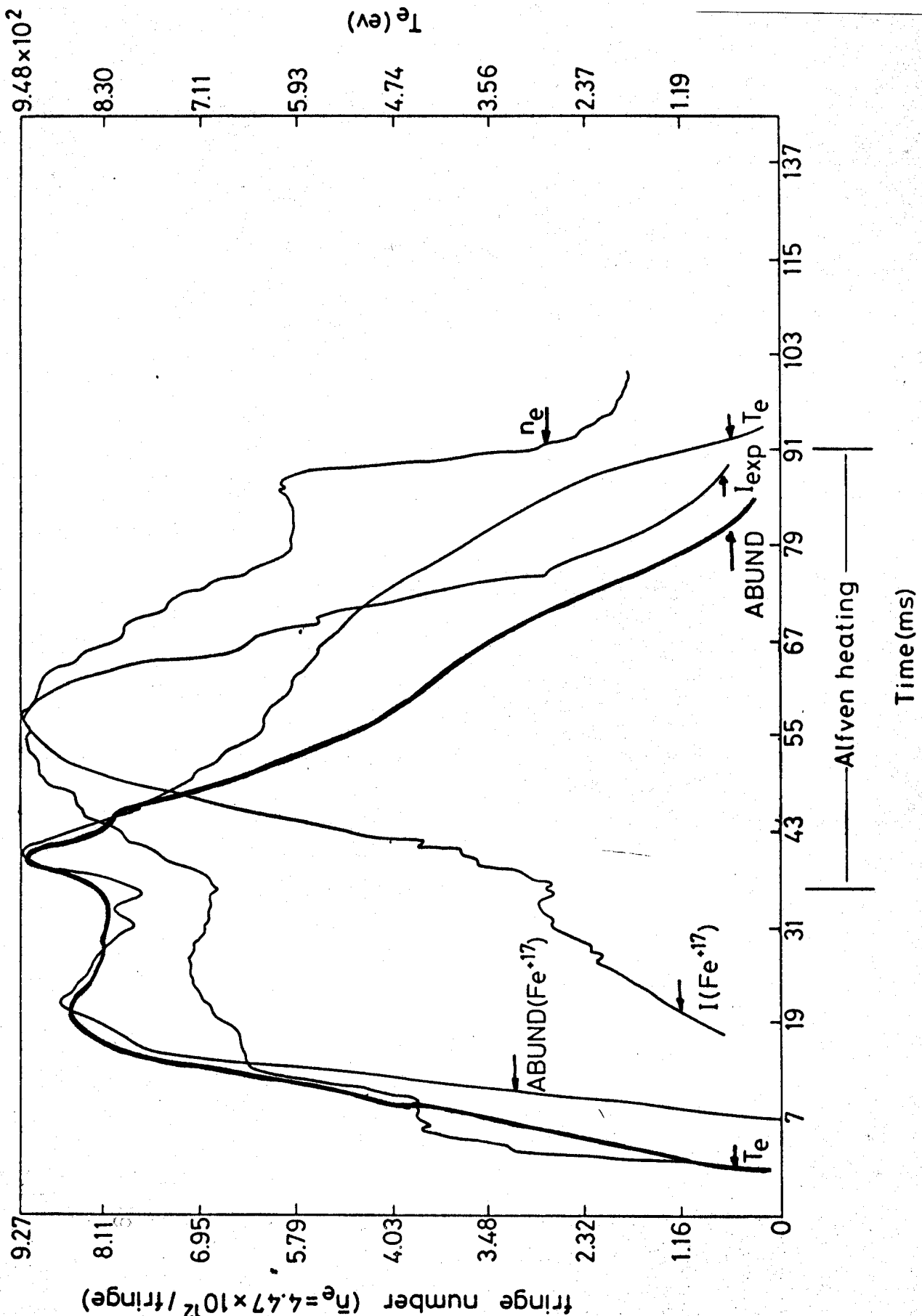

Fig. 13 Comparison between the observed behaviour of the Fe XVIII emission intensity during the rf pulse, and that calculated on the assumption of constant central iron concentration.

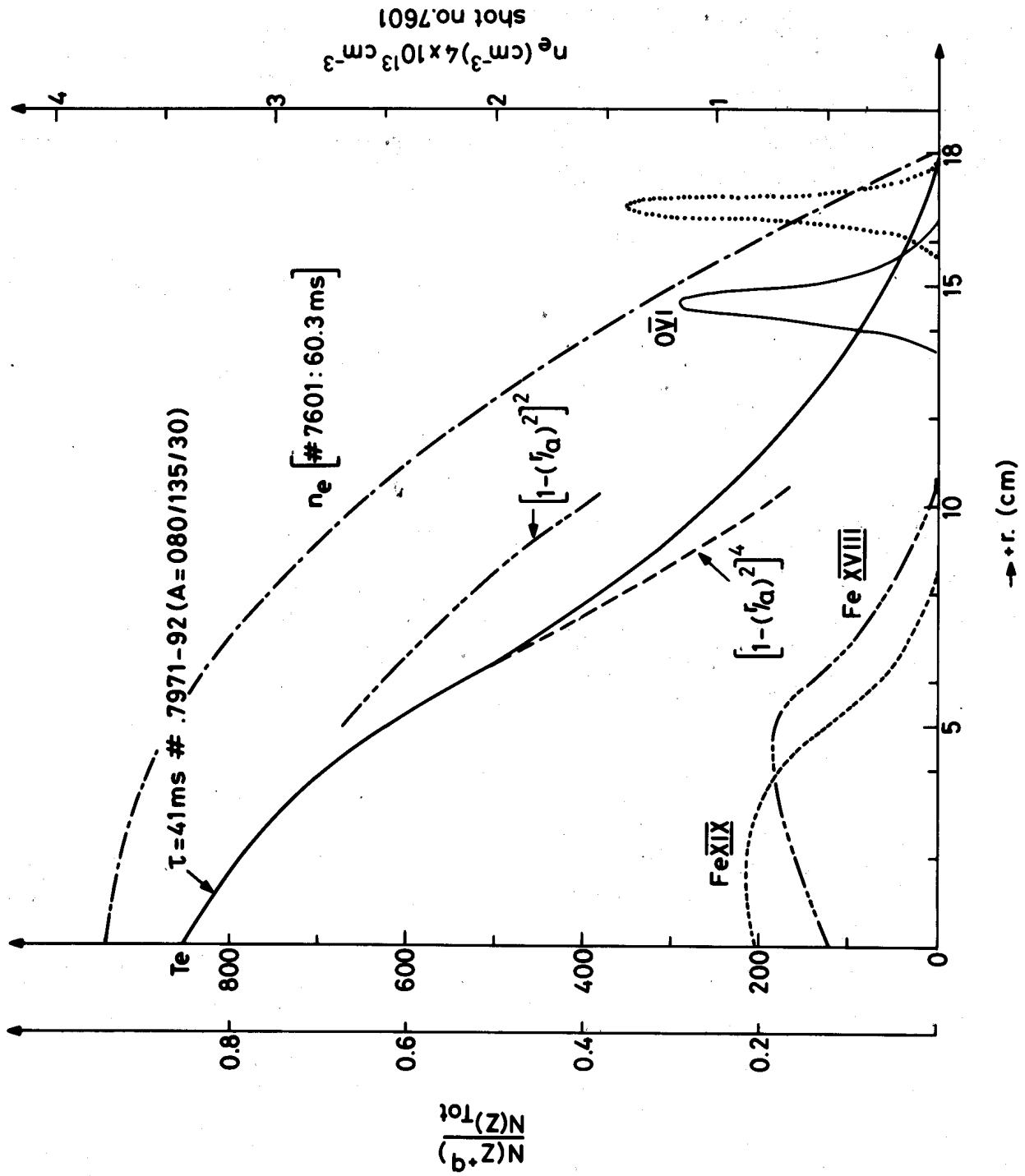

Fig. 14 Ionic radial distribution calculated from the coronal equilibrium for the core ions and a fixed inward diffusion term of 10^4 cm/sec for peripherical ions.

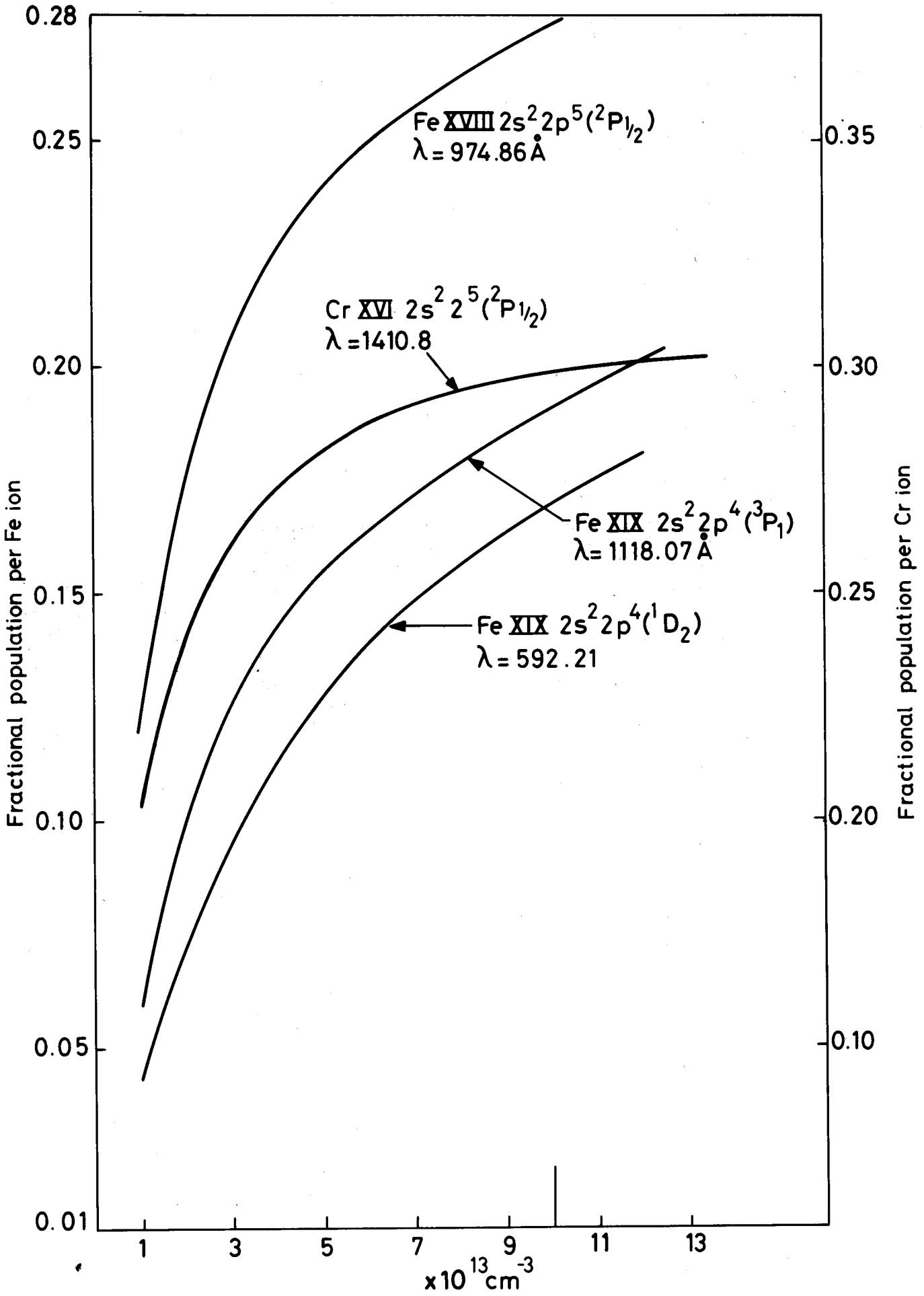

Fig. 15 Dependence of the forbidden line intensities on the plasma